Protonmotive Force: Development of Electrostatic Drivers for Synthetic Molecular Motors

James D. Crowley, Ian M. Steele, and Brice Bosnich*[a]

Abstract: Ferrocene has been investigated as a platform for developing protonmotive electrostatic drivers for molecular motors. When two 3-pyridine groups are substituted to the (rapidly rotating) cyclopentadienyl (Cp) rings of ferrocene, one on each Cp, it is shown that the (Cp) eclipsed, π-stacked rotameric conformation is preferred both in solution and in the solid state. Upon quaternization of both of the pyridines substituents, either by protonation or by alkylation, it is shown that the preferred rotameric conformation is one where the pyridinium groups are rotated away from the fully π-stacked conformation. Electrostatic calculations indicate that the rotation is caused by the electrostatic repulsion between the charges. Consistently, when the π-stacking energy is increased π-stacked population increases, and conversely when the electrostatic repulsion is increased π-stacked population is decreased. This work serves to provide an approximate estimate of the amount of torque that the electrostatically driven ferrocene platform can generate when incorporated into a molecular motor. The overall conclusion is that the electrostatic interaction energy between dicationic ferrocene dipyridyl systems is similar to the π-stacking interaction energy and, consequently, at least tricationic systems are required to fully uncouple the π-stacked pyridine substituents.

Keywords: electrostatic interactions · molecular motors · molecular switches · protonmotive rotation · supramolecular chemistry

Introduction

Biological molecular motors are crucial for the functioning and organization of living systems. These motors can transport cellular material along microtubules or actin filaments,[1] can catalyze the production of ATP by proton-induced rotation,[2] and are responsible for locomotion in living things.[3] In most cases the motors are driven by the hydrolysis of ATP. Unlike macroscopic motors, molecular motors operate by two mechanisms,[4] the "power stroke" where movement is induced by a potential gradient and the "Brownian ratchet" where stochastic Brownian motion is rectified to cause net coherent motion. Biological motors are complex molecular systems and attempts to develop synthetic analogues present challenges of considerable complexity. Even so, progress has been made in devising systems that are driven by protonmotive,[5] electronmotive,[6] and photonmotive[7] forces. The types of systems employed are wide ranging.[8] Herein we describe a systematic study of what might be regarded as drivers (engines) for potential molecular motors and machines. For this purpose we have elaborated the ferrocene molecule and have exploited the rotation of the cyclopentadienyl (Cp) rings for induced rotary motion.

Results and Discussion

The [Fe(Cp)$_2$]-based driver: Ferrocene, **1**, is a stable molecule, it prefers an eclipsed conformation of its Cp rings,[9,10] **2**, the distance between the Cp rings is 3.298 Å,[11] and the barrier to rotation of the Cp rings is 0.9(3) kcal mol^{-1}.[9,12] As

[a] Dr. J. D. Crowley, Dr. I. M. Steele, Prof. B. Bosnich
Department of Chemistry
The University of Chicago
5735 South Ellis Avenue, Chicago, IL 60637 (USA)
Fax: (+1)773-702-0805
E-mail: bos5@uchicago.edu

eclipsed   staggered

1   **2**

WILEY InterScience®
DISCOVER SOMETHING GREAT
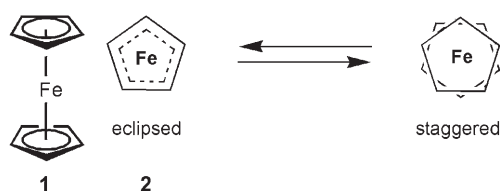
a consequence of the low rotational barrier, the Cp rings are in rapid rotation even at very low temperatures. Inspection of crystal structures of 1,1′-diarylsubstituted ferrocenes[13] reveals that in nearly all of the cases the Cp rings are eclipsed and the aryl groups on the Cp rings are π-stacked. This π-stacking also obtains in solution.[14, 15] Aromatic π–π stacking occurs at distances of 3.30 to 3.50 Å.[16] This distance span is slightly greater than the interplanar Cp–Cp separation (3.298 Å), nonetheless, π–π stacking of 1,1′-diaryl ferrocenes is almost universally observed.

To convert ferrocenes into electrostatic drivers, we chose 1,1′-substitution by basic aromatic groups, which are neutral but which can be made positively charged by quarternization or by protonation. The basic idea is outlined by **3** and **4**. The molecule **3** is expected to prefer the Cp rings in an
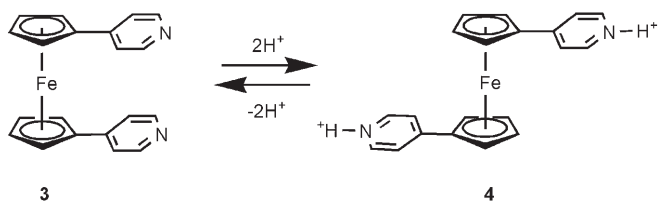

eclipsed conformation and the pyridine groups π-stacked as shown. Upon addition of acid, the pyridine groups will become protonated. As a consequence, electrostatic repulsion between the two positively charged pyridine groups will cause the Cp rings to rotate and adopt an orientation that minimizes the Coulombic interaction. We, however, have found for both ferrocene- and ruthenocene-substituted systems that if a basic ring nitrogen atom is positioned such that the Cp ring can conjugate to form a fulvene structure when the nitrogen is protonated, the complexes become unstable in acid solution. An example of this conjugation is shown in **6**.[17] (Protonation of the [FeCp$_2$] iron atom does
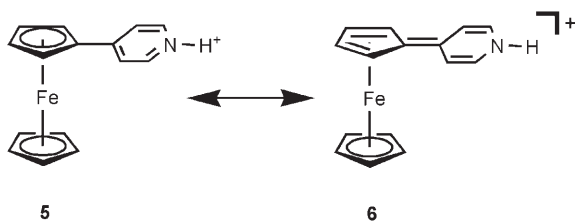
not occur in acetonitrile solutions even with 100-fold excess of trifluoroacetic acid as evidenced by ^{1}H NMR spectra.[18]) Thus the electrostatic drivers discussed here are ferrocene systems bearing aromatic substituents which cannot engage in the proton-induced conjugative shift that leads to decomposition.

Electrostatic interactions: The essential elements of the electrostatic drivers can be illustrated by the assumed behavior of 1,1′-di-3-pyridylferrocene, **7**, in the (drawn) *meso* conformation. Rotation of ferrocene itself will produce a sinusoidal energy profile where there are five wells of a depth

of about 1 kcal mol^{-1} that refer to the (five degenerate) eclipsed conformations. For the molecule **7**, it is assumed that the two pyridine groups will π-stack (in the eclipsed Cp conformation). Calculations[19] and
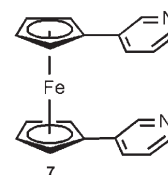
experiments[20] indicate that a pair of symmetrically disposed face-to-face π-stacked benzene molecules is stabilized by about 2 kcal mol^{-1}. Thus, assuming a similar value for two π-stacked pyridine groups, the total well depth for the Cp-eclipsed π-stacked rotamer of **7**, is about 3 kcal mol^{-1}. Although it is probably correct to assume a sinusoidal variation for the pure Cp rotation,[12] it is not clear what the shape of the energy well for the π–π stacking is when the two pyridine groups are rotated (parallel) with respect to each other. Although a complex function probably obtains for this process, we have used a sine function whose depth is 2 kcal mol^{-1} at the eclipsed π-stacked rotamer and whose half wave encompasses plus 108° to minus 108° rotation of the Cp rings from the energy minimum (see Supporting Information). The energy well was extended to ±108° of Cp rotation because at smaller rotations, the two pyridine substituents overlap with each other to varying degrees. Addition of the two rotational functions, one for Cp rotation and the other for π–π interaction, gives the energy profile for Cp rotation of **7**. This is shown as the lower curve in Figure 1.

Whereas the neutral compound **7** and its analogues are soluble in solvents of low dielectric constant such as CH$_2$Cl$_2$, upon quaternization they become insoluble in these solvents with the SbF$_6^-$ counter ion. The SbF$_6^-$ ion was used to avoid hydrogen bonding between the counter ion and the protonated pyridine groups. Acetone and acetonitrile are good solvents for both the neutral and charged species. To obtain an estimate of the electrostatic repulsion in these two solvents, the Coulombic energy was calculated by using the (bulk) dielectric constant of acetone (20.2) and acetonitrile (36.2) for diprotonated **7**. When the pyridinium groups are stacked, the effective dielectric constant is likely to be lower than that of the bulk solvent because the charges are partly screened by the aromatic rings. As rotation away from the stacked rotamer increases, the solvent dielectric constant is likely to become more realistic. Point charges located on the nitrogen atoms were used and the separations between the charges were calculated by rotating the pyridinium groups while retaining their coplanar relationship. As we show by NOE experiments later, the pyridine (and pyridinium) substituents rotate about the single bond that connects them to the Cp rings. It was possible to include such rotation in the calculation but such detail did not seem to provide anything new associated with these electrostatic drivers.

Figure 1 shows the Coulombic repulsion that is calculated for Cp ring rotation in acetonitrile and acetone solutions for the diprotonated *meso* rotamer of **7**. Addition of these Coulombic plots to the (lower) Cp-rotation-π–π-stacking plot gives the two curves shown in Figure 1. Rotation occurs in
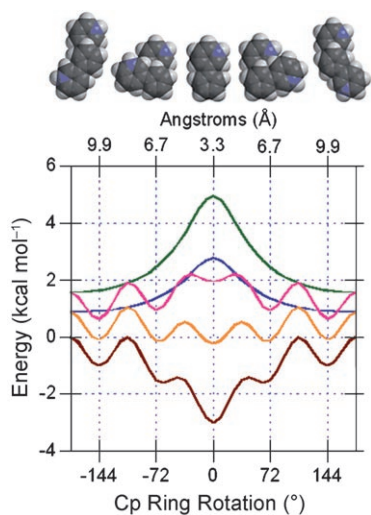
Figure 1. The calculated electrostatic repulsion curves for the meso rotamer in acetonitrile (——) and acetone (——) solutions. The calculated energy profile for the ferrocene Cp rotation (——). The sum of the Cp rotation and the electrostatic repulsion in acetonitrile (——), and in acetone (——). The nitrogen–nitrogen distance at 0° is 3.30 Å. The maximum electrostatic repulsion energy is 2.77 kcal mol^{-1} in acetonitrile and 4.96 kcal mol^{-1} in acetone. The space-filling models show the rotation of the two protonated 3-pyridine groups for the angles shown in the lowest ordinate.
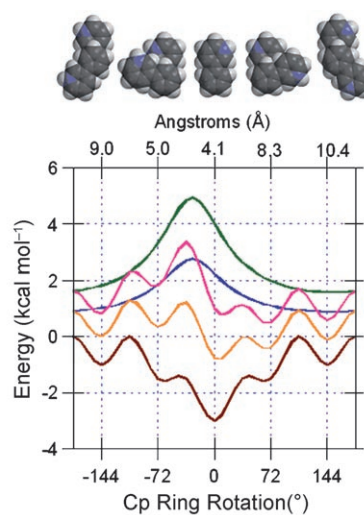

Figure 2. The calculated electrostatic repulsion curves for a racemic rotamer in acetonitrile (——) and acetone (——) solutions. The calculated energy profile for the ferrocene Cp rotation (——). The sum of the Cp rotation and the electrostatic repulsion in acetonitrile (——), and in acetone (——). The nitrogen–nitrogen distance at 0° is 4.10 Å. The maximum electrostatic repulsion energy is 2.77 kcal mol^{-1} in acetonitrile and 4.96 kcal mol^{-1} in acetone. The space-filling models show the rotation of the pyridinium groups for the angles shown in the lowest ordinate.

either direction with the same energy as expected for the (achiral) *meso* rotamer. Inspection of the resultant energy profile in acetonitrile solution shows that there is little or no preference for any rotamer. Shallow energy wells of about the same depth occur at the eclipsed Cp conformations. The analogous energy profile for acetone solution indicates that rotation of the pyridinium groups will occur either to the $\pm 72°$ or $\pm 144°$ wells. At the present level of calculation, the results suggest that in acetone or solutions with lower dielectric constants, electrostatic repulsion is likely to cause rotation of the pyridinium groups. For the *meso* rotamer, the present approximate calculations do not predict that the pyridinium groups will be significantly rotated in acetonitrile solutions when each of the pyridinium groups carries one (positive) charge each. For the interaction of a 2+ group with a 1+ group, these calculations would predict rotation. As noted, however, the solvent bulk dielectric constant may not be an appropriate constant when the groups are π-stacked, and as experiments here show, some rotation of the pyridinium groups obtains in acetonitrile solutions.

Figure 2 shows the analogous curves for one enantiomer of the racemic rotamer of **7**. There are two features of interest shown by these energy relationships. First, the profile is unsymmetrical. As a consequence, rotation of the pyridinium groups is biased in one direction; biased clockwise for one enantiomer and biased counterclockwise for the other. Second, in acetonitrile solution the pyridinium groups will rotate and prefer to lie oriented at an angle of less than 72° according to these calculations. In acetone solution, the pyridinium groups will rotate further than in acetonitrile and will lie either at ≈70° or at ±144° according to these calcu-

lations. A similar situation as found for the acetone solution obtains for the interaction of a 2+ with 1+ interaction in acetonitrile solution.

A consideration of the energy curves in Figure 1 and Figure 2 suggests that generally there exist energy wells in the racemic rotamer that are more stable than those of the *meso* pyridinium rotamer. It should, however, be emphasized that the variation in energy for any composite curve is small and detailed discussion is circumscribed by the approximate nature of the calculations.

Synthesis: The synthesis of the symmetrical and unsymmetrical 1,1′-diaryl ferrocenes followed the excellent procedures reported by Braga.[21,22] The details are given in the experimental section and are summarized in Equations (1) to (7) in Scheme 1. The Suzuki couplings proceed in moderate to good yields. It was found that mono-substitution of the diboronic acids proceeds best by short microwave induction. Addition of the second substituent to the monoboronic acid was found to give the best yields under standard Suzuki conditions. Using acetone as a solvent, AgSbF$_6$ removal of the chloro ligands from the palladium complex in Equation (5) in the presence of pyridine, yields two products; one is the dipyridine complex (75% yield) and the other is the monopyridine complex, which has the other coordination position occupied by a σ-bonded carbon atom of the acetone anion (15% yield). This latter complex is presumably formed after acetone is deprotonated by pyridine. The two products in Equation (5) are separated by crystallization.

The preparation of 3-bromo-8-nitroquinoline [Eq. (6)] has been described[23] but the two nitro isomers were misassigned; the minor component is the 8-nitro isomer. This is
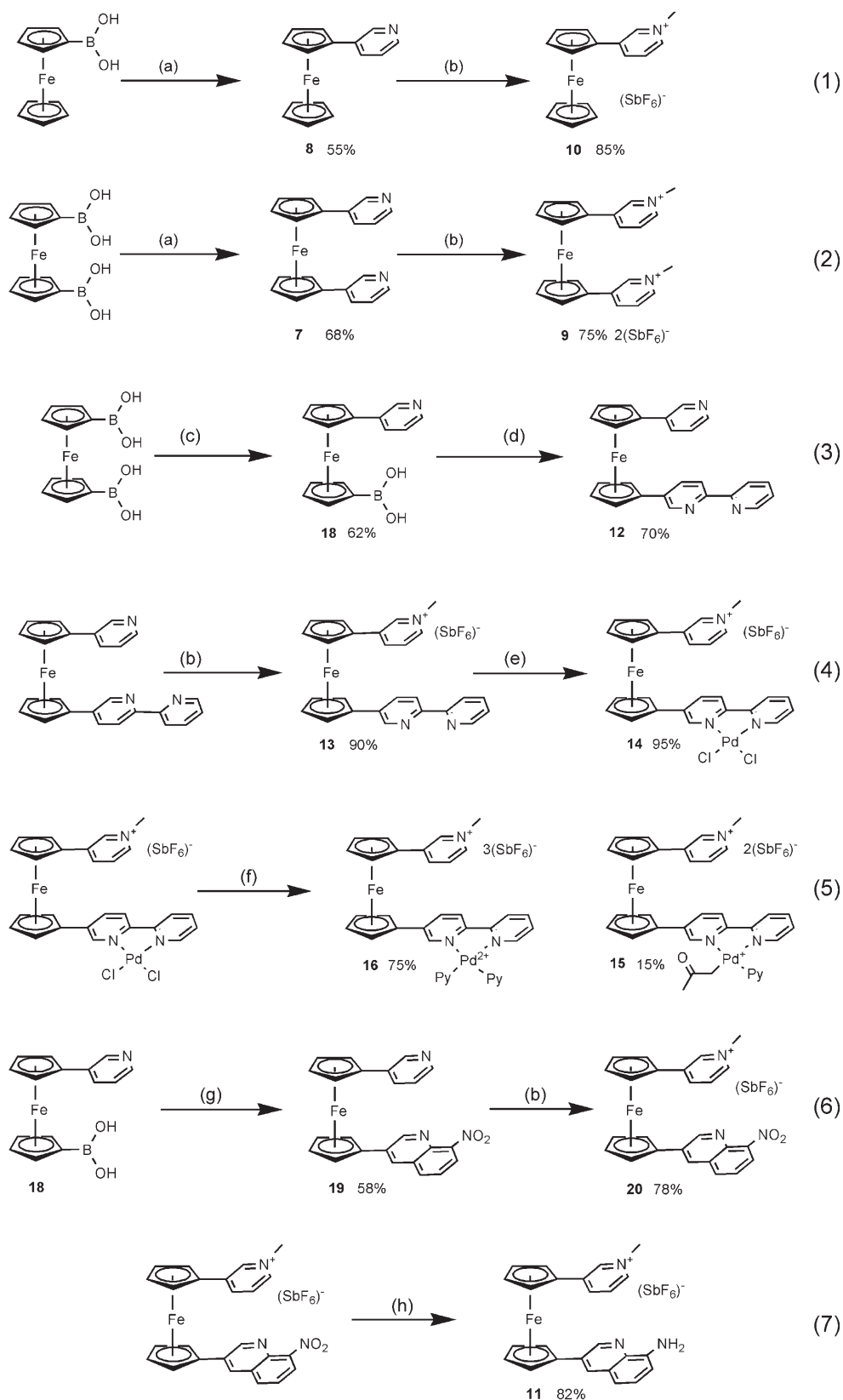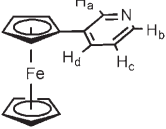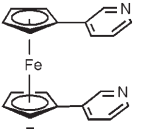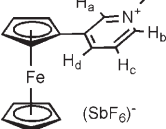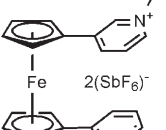
Scheme 1. a) 3-bromopyridine, Na₂CO₃, dioxane, NaOH (aq), DME, [Pd(dppf)Cl₂], 100°C, 24 h; b) i) CH₃I, CH₂Cl₂, RT, 16 h; ii) AgSbF₆, acetone, RT, 1 h; c) 3-bromopyridine, Na₂CO₃, dioxane, NaOH (aq), DME, [Pd(dppf)Cl₂], reflux, microwave, 12 min; d) 5-bromo-2,2′-bipyridine, Na₂CO₃, dioxane, NaOH (aq), DME, [Pd(dppf)Cl₂], 100°C, 20 h; e) [Pd(NCCH₃)₂Cl₂], acetone, RT, 1 h; f) i) 2 equiv AgSbF₆, acetone RT, 1 h; ii) 2 equiv pyridine (Py), acetone, RT, 1 h; g) 3-bromo-8-nitroquinoline, Na₂CO₃, dioxane, NaOH (aq), DME, [Pd(dppf)Cl₂], 100°C, 24 h; h) NH₂NH₂, graphite, EtOH/CH₃CN, reflux 36 h. dppf = 1,1′-diphenylphosphinoferrocene, DME = dimethoxyethane.

confirmed by X-ray diffraction (see later). Reduction of the nitro group to the amine is efficiently carried out by the graphite/hydrazine ethanol procedure.[24] All of these compounds are conveniently stable both as solids and in solution.

The 1,1′pyridylferrocene systems: The four systems investigated were **7**, **8**, **9**, and **10** (Table 1). The monosubstituted

Table 1. Chemical shifts of the protons of the pyridine substituents of various ferrocene compounds in [D$_3$]acetonitrile solutions.

Compound	Chemical shift (δ)			
	H$_a$	H$_b$	H$_c$	H$_d$
8	8.73	8.38	7.24	7.86
7	8.46	8.28	7.01	7.48
difference ($\Delta\delta$)	−0.27	−0.10	−0.23	−0.38
10	8.63	8.45	7.83	8.34
9	8.55	8.38	7.76	8.24
difference ($\Delta\delta$)	−0.08	−0.07	−0.07	−0.10

compounds **9** and **10** were used to determine the chemical shifts of the protons on the pyridine rings when no π-stacking is present. In the disubstituted cases **7** and **8** π-stacking is expected to induce (upfield) chemical shifts[14,15] of the pyridine protons. Although these compounds are highly fluxional, the chemical shifts for the disubstituted species **7** and **8** are related to the concentration weighted sum of the chemical shifts of all of the possible rotamers. Thus, for example the greater the average concentration of the π-stacked rotamers, the greater the upfield shift of the signal for any proton in the ^{1}H NMR spectrum. The absence of π-stacking would be indicated by chemical shifts that are the same as for the corresponding monomers.

The chemical shifts of the pyridine protons of **8** and **7** in [D$_3$]acetonitrile solutions and the corresponding differences in chemical shifts are listed in Table 1. It will be noted that in acetonitrile solutions all of the pyridine protons in **7** expe-

rience an upfield chemical shift compared to those of **8**, indicating that the pyridine substituents of **7** are π-stacked at least to some extent. A similar comparison of **9** with **10** indicates that the pyridinium groups of **9** are not extensively π-stacked because of the small differences in chemical shift ($\Delta\delta$) for the two compounds. That the neutral compound **7** is π-stacked to a greater extent than the charged analogue **9** is consistent with the electrostatic arguments presented earlier.

For these ferrocene systems to act as protonmotive drivers, compound **7** should rotate from its eclipsed π-stacked rotameric configuration upon protonation of the pyridine groups. Two acids were used: CF$_3$CO$_2$H, which is not dissociated in dry acetonitrile[25] and HSbF$_6$·6H$_2$O which, in acetonitrile solutions, was found to be highly conducting, suggesting dissociation of the proton from SbF$_6^-$.
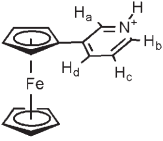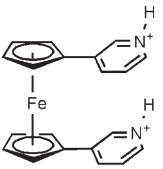
The protonation of **7** and **8** with CF$_3$CO$_2$H in dry acetonitrile was studied by examination of ^{1}H NMR spectral shifts of the pyridine protons. Five equivalents of CF$_3$CO$_2$H were required to fully protonate **8** as indicated by the chemical shifts becoming insensitive to further addition of acid. Conductivities of 10^{-3} M solutions of fully protonated **8** were 165 Ω^{-1}cm^{2}mol^{-1}, which is that expected for a 1:1 electrolyte in acetonitrile solution (120–160 Ω^{-1}cm^{2}mol^{-1}).[26] Hence the protonated form of **8** appears to be fully dissociated in acetonitrile solution with the CF$_3$CO$_2^-$ counterion. A similar titration with CF$_3$CO$_2$H and the dipyridine system, **7**, required 10 equivalents of CF$_3$CO$_2$H for full protonation (see Supporting Information). The conductivity in acetonitrile for a 10^{-3} M solution of the protonated form of **7** was 208 Ω^{-1}cm^{2}mol^{-1}, which is slightly lower than expected for a 2:1 electrolyte in dry acetonitrile (220–300 Ω^{-1}cm^{2}mol^{-1}).[26] The much stronger acid HSbF$_6$·6H$_2$O fully protonated **8** and **7** upon the addition of 1 and 2 equivalents of HSbF$_6$·6H$_2$O to the 10^{-3} M acetonitrile solutions, respectively.

Table 2 lists the chemical shifts for the two protonated systems at 25°C. The two acids cause almost the same proton chemical shifts for the two compounds. The chemical shift differences ($\Delta\delta$) are also similar for the two acids, with $\Delta\delta$ for the CF$_3$CO$_2$H protonation being larger in magnitude. This may suggest that HSbF$_6$·6H$_2$O is most effective in uncoupling the π-stacking.

The solid-state structures of five compounds bearing only 3-pyridine or pyridinium substituents were determined by X-ray crystallography to try to obtain a more detailed understanding of the structures. We were unable to obtain a structure of the neutral di-3-pyridine compound **7**, because the crystals were always twinned, even after crystallization from several solvent combinations. Based on the work of Braga et al.[22] and the present studies, there seems little doubt that the two pyridine groups of **7** are π-stacked.

Figure 3 and Figure 4 show two perspectives of the structures of **10** and **9** as their SbF$_6^-$ salts. Table 3 lists the appropriate crystallographic data. The bond lengths and angles are unexceptional. The information germane to the present study is summarized in Table 4. The present structures and

Table 2. Chemical shifts of the protons of the pyridinium substituent of the mono- and disubstituted ferrocenes in [D$_3$]acetonitrile solutions when protonated by CF$_3$CO$_2$H and HSbF$_6\cdot$6H$_2$O.

Compound	Chemical shift (δ)							
	CF$_3$CO$_2$H				HSbF$_6\cdot$6H$_2$O			
	H$_a$	H$_b$	H$_c$	H$_d$	H$_a$	H$_b$	H$_c$	H$_d$
8 (H$^+$)	8.66	8.58	8.44	7.86	8.66	8.60	8.42	7.88
7 (H$^+$)$_2$	8.46	8.40	8.24	7.66	8.50	8.46	8.32	7.76
difference ($\Delta\delta$)	−0.20	−0.18	−0.20	−0.20	−0.16	−0.14	−0.10	−0.12

the CF$_3$CO$_2$H and CF$_3$SO$_3$H derived salts one pyridinium group is protonated but hydrogen-bonded to either the CF$_3$CO$_2^-$ or CF$_3$SO$_3^-$ group, whereas the other pyridinium group is also protonated but is not hydrogen-bonded. Thus, because of the hydrogen-bonding in the crystal, one pyridinium group is essentially neutral while the other is positively charged. That the pyridinium groups are π-stacked in these cases, is no surprise.

To avoid the effects of hydrogen-bonding on the rotamer configuration in the solid, we have employed the SbF$_6^-$ salts, which are not expected to hydrogen-bond. The di-quaternary methyl compound, **9**, was also investigated in order to see if similar structures were
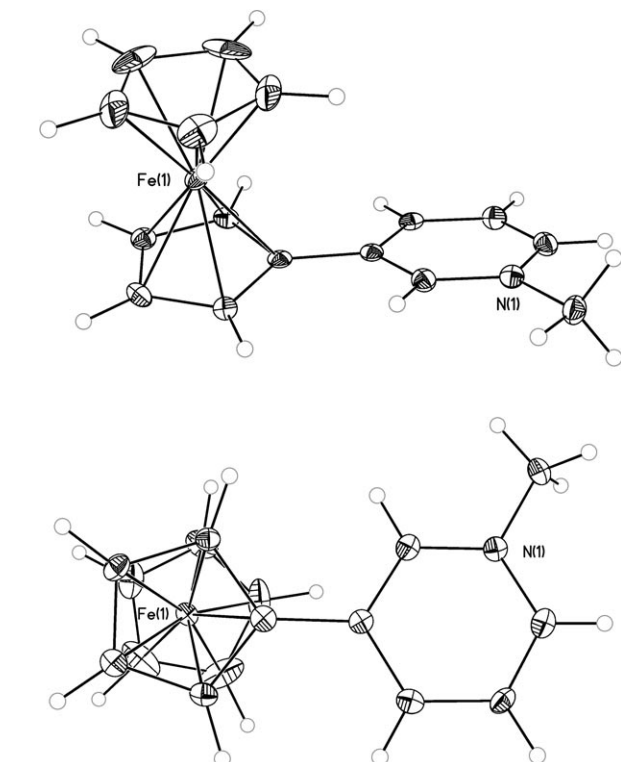

Figure 3. Two perspectives of the solid-state structure of **10** as the SbF$_6^-$ salt. Thermal ellipsoids are at 50 % probability. The hydrogen atoms shown are calculated, they were not located. The SbF$_6^-$ ion is omitted for clarity.

those reported bearing one aromatic ring on each Cp ring have the aromatic rings roughly coplanar with the Cp ring to which it is attached.

The diprotonated salts of **7** formed from CF$_3$COOH and CF$_3$SO$_3$H, form crystals that contain molecules that have the pyridinium substituents eclipsed (see Figure 12 and Figure 13 in the Supporting Information). For the cases of
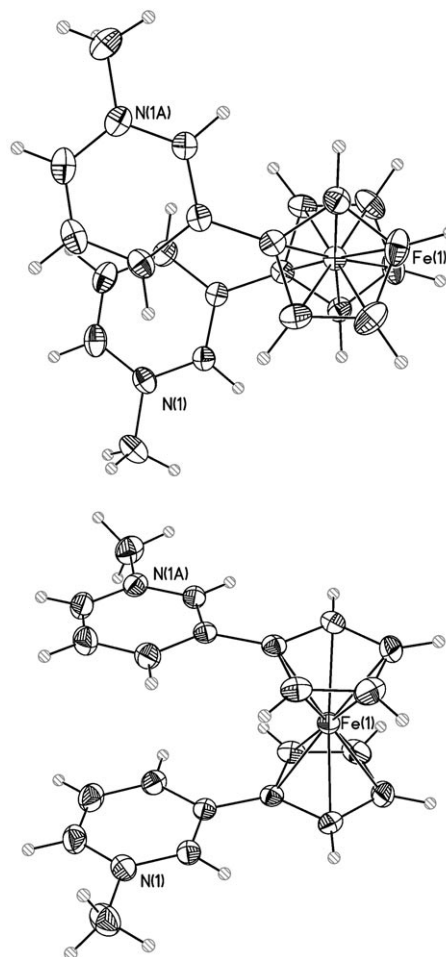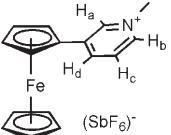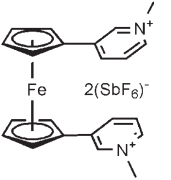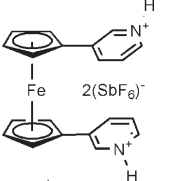

Figure 4. Two perspectives of the solid-state structure of **9** as the SbF$_6^-$ salt. Thermal ellipsoids are at 50 % probability. The hydrogen atoms shown are calculated, they were not located. The SbF$_6^-$ ions are omitted for clarity.

Table 3. Crystallographic data for **7**·2(HSbF$_6$), **9**, and **10**.

Compound	**7**·2(HSbF$_6$)	**9**	**10**
formula	C$_{20}$H$_{18}$FeN$_2$ + 2(SbF$_6$) + C$_2$H$_6$O	C$_{22}$H$_{22}$FeN$_2$ + 2SbF$_6$	C$_{20}$H$_{18}$FeN$_2$ + SbF$_6$
formula weight	840.78	830.68	513.90
space group	$P\bar{1}$	C2/c	C2/c
a [Å]	7.341(8)	18.055(3)	20.865(5)
b [Å]	10.439(11)	11.654(2)	6.3412(14)
c [Å]	18.683(19)	13.251(3)	27.133(6)
α [°]	89.914(16)	90.0 (3)	90.0
β [°]	80.141(17)	107.755(3)	110.312(4)
γ [°]	71.143(15)	90.0 (3)	90.0
V [Å^3]	1333(2)	2655.3(8)	3366.7(13)
Z	2	4	8
cryst. size	0.20×0.10×0.03 mm	0.20×0.20×0.15 mm	0.17×0.15×0.04 mm
color, habit	red, needle	red, fragment	red-orange, plate
ρ_{calcd}, g [cm^{-3}]	2.095	2.078	2.028
μ [mm^{-1}]	2.647	2.658	2.527
T [K]	221(2)	100(5)	100(5)
wavelength [Å]	0.71073 (Mo$_{K\alpha}$)	0.71073 (Mo$_{K\alpha}$)	0.71073 (Mo$_{K\alpha}$)
R(F) [%][a]	11.56	3.67	5.09
R(wF^2) [%][a]	26.73	10.17	8.64

Table 4. Important angles and distances for several pyridine or pyridinium substituted ferrocenes.

Compound	Angles			Distance
	Cp–Cp [°][a]	Cp–Py$_1$ [°][b]	Cp–Py$_2$ [°][b]	Py–Py [Å][c]
10	10.85	14.7	–	–
9	37.52	4.10	4.10	3.34
7 (H$^+$)$_2$	29.62	5.8	6.7	3.28

[a] Cp–Cp rotation angle; eclipsed angle is 0°. [b] Interplanar angle between Cp and Py rings. [c] Average interplanar separation between the pyridine rings.

obtained in the solid state for two different quaternized SbF$_6^-$ salts (Figure 4 and Figure 5). Both solid state structures have the substituents rotated away from the eclipsed π-stacked rotamer. Both structures are in the racemic conformation. The Cp–Cp rotations are similar, 29.62° and 37.52° for **7**(H$^+$)$_2$ and **9**, respectively. In both cases some π–π overlap occurs. Assuming that crystal packing forces are

not dominant in deciding the rotamer configurations in these cases, the small Cp–Cp rotation angle suggests that the Coulombic repulsion and eclipsed π-stacking forces are similar in energy. The solution ^{1}H NMR spectral data and the calculations shown in Figure 1 and Figure 2 are also consistent with the conclusion that the repulsive and stabilizing forces are of a similar magnitude. The π–π-stacking distances py–py (Table 4) are within the range expected for such interactions.

If the stabilizing forces in the eclipsed π-stacked rotamer are of similar energy to the electrostatic forces for the dipyridinium systems, then it follows that if the π–π attractive forces were increased to a modest degree, the electrostatic repulsion may not be sufficient to overcome the stabilizing forces. This was investigated for the methylpyridinium and 8-aminoquinolyl combination, **11**.

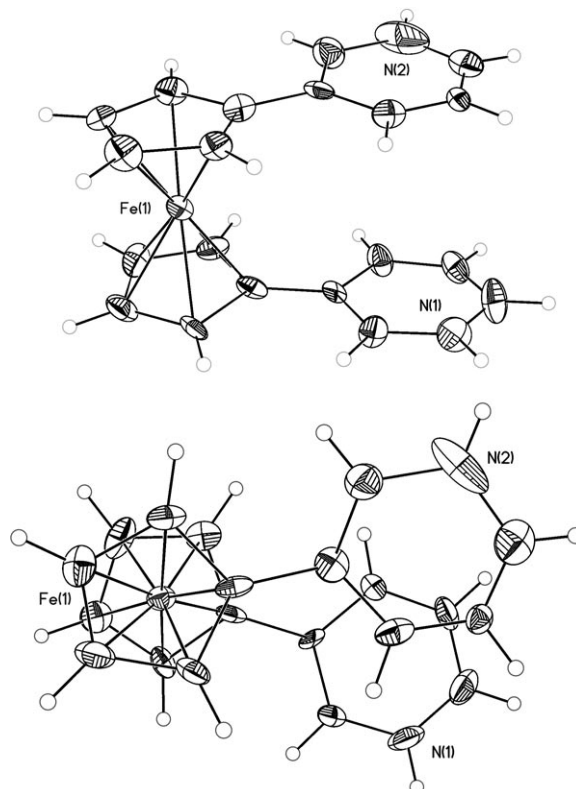Figure 5. Two perspectives of the solid-state structure of **7**(H$^+$)$_2$ as the SbF$_6^-$ salt. Thermal ellipsoids are at 50% probability. The hydrogen atoms shown are calculated, they were not located. The SbF$_6^-$ ions are omitted for clarity.
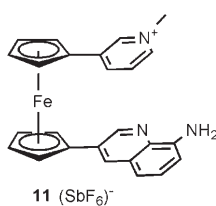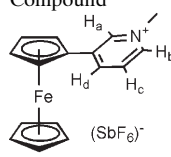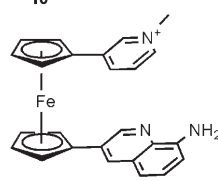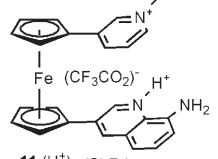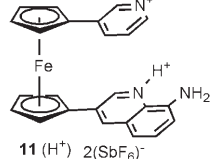
11 (SbF$_6$)$^-$

Table 5 lists the pyridine proton chemical shifts and chemical shift differences ($\Delta\delta$) for free monoprotonated **11** in acetonitrile solution as well as those for the reference molecule **10**. It was found that 60 equivalents of CF$_3$CO$_2$H were required to fully monoprotonate **11** and that 10 equivalents of HSbF$_6$·6H$_2$O were necessary to achieve full monoprotonation of **11** (see Supporting Information). The large number of acid equivalents

The *N*-methylpyridinium group can be regarded as electron-poor, whereas the 8-aminoquinoline group is electron-rich; this, together with the greater π-surface of the latter should lead to greater π–π interaction than when the quinoline group is replaced by a pyridine moiety. As can be seen in Table 5, the chemical shift differences ($\Delta\delta$) between **10** and **11** are much larger than observed for difference between the mono- **8**, and dipyridine **7** analogues. This suggests a greater π-stacked population for **11** than for **7**, consistent with the assumption that **11** will have a greater π–π interaction energy.

The two monoprotonated complexes, **11** (H$^+$), one derived from CF$_3$CO$_2$H and the other from HSbF$_6$·6H$_2$O protonation, have essentially the same $\Delta\delta$ values, suggesting that both acids fully protonate **11** without significant ion-pairing. The magnitudes of the shifts clearly indicate that, on average, the two groups are not fully separated and that there exist significant populations of π-stacked species.

The crystal structures of **11** and the monoprotonated form **11**(H$^+$) both as SbF$_6$$^-$ salts were determined. The crystallographic data are listed in Table 6 and the structures are shown in Figure 6 and Figure 7 in two orientations. The salient parameters are listed in Table 7.

Table 5. Chemical shifts of the protons of the *N*-methylpyridinium substituents in [D$_3$]acetonitrile solutions for the compounds **10** and **11** and for CF$_3$CO$_2$H and HSbF$_6$·6H$_2$O monoprotonation of **11**.

| Compound | Chemical shift (δ) | | | |
	H$_a$	H$_b$	H$_c$	H$_d$
10	8.63	8.45	7.83	8.34
11 (SbF$_6$)$^-$	7.89	7.71	6.97	7.45
difference ($\Delta\delta$)	−0.74	−0.74	−0.86	−0.89
11 (H$^+$) (SbF$_6$)$^-$	8.37[a]	7.99[a]	7.35[a]	7.93[a]
difference ($\Delta\delta$)	−0.26	−0.46	−0.48	−0.41
11 (H$^+$) 2(SbF$_6$)$^-$	8.37[b]	7.98[b]	7.34[b]	7.94[b]
difference ($\Delta\delta$)	−0.26	−0.47	−0.49	−0.40

[a] CF$_3$CO$_2$H. [b] HSbF$_6$·6H$_2$O.

Table 6. Crystallographic data for **11** and the **11**·HSbF$_6$.

Compound	**11**	**11**·HSbF$_6$
formula	C$_{25}$H$_{22}$FeN$_3$ + SbF$_6$	C$_{24}$H$_{23}$FeN$_3$ + H$_2$O + 2SbF$_6$
formula weight	656.06	889.81
space group	$P2_12_12_1$	$P\bar{1}$
a [Å]	7.478(2)	10.348(20)
b [Å]	15.871(5)	10.69(2)
c [Å]	19.594(6)	14.03(3)
α [°]	90.0	70.44(3)
β [°]	90.0	81.60(3)
γ [°]	90.0	69.69(3)
V [Å^3]	2325.3(12)	1347(4)
Z	4	2
cryst. size	0.25 × 0.15 × 0.03 mm	0.30 × 0.20 × 0.10 mm
color, habit	red, plate	black, plate
ρ_{calcd} [g cm^{-3}]	1.874	2.155
μ [mm^{-1}]	1.854	2.580
T [K]	100(5)	100(5)
wavelength [Å]	0.71073 (Mo$_{K\alpha}$)	0.71073 (Mo$_{K\alpha}$)
$R(F)$ [%][a]	3.31	10.30
$R(wF^2)$ [%][a]	7.42	27.28

[a] Quantity minimized $= R(wF^2) = \Sigma[w(F_o^2 - F_c^2)^2]/\Sigma[(wF_o^2)^2]^{1/2}$; $R = \Sigma\Delta/\Sigma(F_o)$, $\Delta = |(F_o - F_c)|$ $w = 1/[\sigma^2(F_o^2) + (aP)^2 + bP]$, $P = [2_c^2 + \text{Max}(F_o, 0)]/3$.

necessary to monoprotonate **11** is, at least in part, connected with the repulsion of the neighboring positive charge on the *N*-methylpyridinium group. That only monoprotonation occurs under these conditions was confirmed by the appearance of isosbestic points for the electronic absorption spectra recorded for various concentrations of acid (see Supporting Information). Further, for the fully protonated complex with CF$_3$CO$_2$H, the conductivity was found to be 209 Ω^{-1} cm^2 mol^{-1} which, as noted, is close to that expected for a 2:1 electrolyte in acetonitrile.

The results illustrated in Figure 6 and Figure 7 and tabulated in Table 7 show that the solid-state structures for **11** and its monoprotonated form **11**(H$^+$) are essentially the same. These observations most probably indicate greater π–π stacking interactions for these compounds as compared to the previous ones. The structure in the solid state, however, is also governed by the exigencies of crystal packing and the coincidental structures may be a reflection of these forces rather than the interplay of electrostatic repulsion forces with those associated with π–π interactions. The ^{1}H NMR
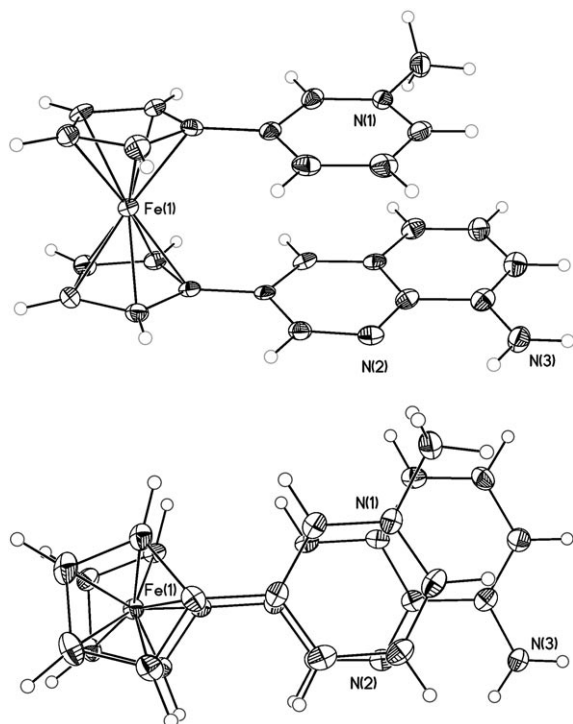
Figure 6. Two perspectives of the solid-state structure of **11** as the SbF_6^- salt. Thermal ellipsoids are at 50% probability. The hydrogen atoms shown are calculated, they were not located. The SbF_6^- ion is omitted for clarity.

Figure 7. Two perspectives of the solid-state structure of **11**(H$^+$)$_2$ as the SbF_6^- salt. Thermal ellipsoids are at 50% probability. The hydrogen atoms shown are calculated, they were not located. The SbF_6^- ions are omitted for clarity.
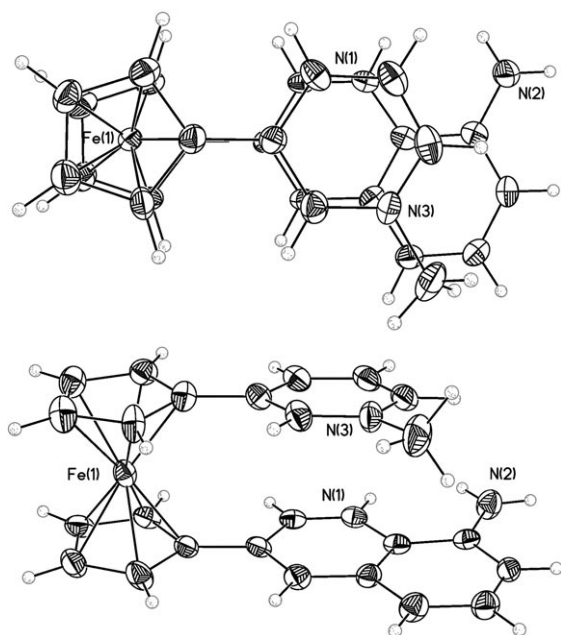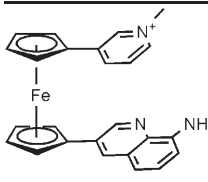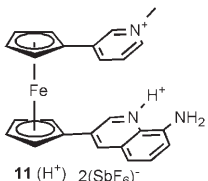
data for **11**(H$^+$), however, clearly indicate that the equilibrium is not completely tilted to the π-stacked rotamer in solution. Thus, crystal structures, although informative, need not

Table 7. Important angles and distances for several pyridine or pyridinium substituted ferrocenes.

| Compound | Angles | | | Distance |
	Cp–Cp [°][a]	Cp–Py [°][b]	Cp–Q [°][b]	Py–Q [Å][c]
11 (SbF$_6$)$^-$	0.52	13.10	8.90	3.28
11 (H$^+$) 2(SbF$_6$)$^-$	1.00	7.40	2.10	3.35

[a] Cp–Cp rotation angle; eclipsed angle is 0°. [b] Interplanar angle between Cp and pyridine (Py) or quinoline (Q) rings. [c] Average interplanar separation between the pyridine and quinoline rings.

necessarily reflect the preferred rotamer especially when salts are involved.

Overall, the preceding data indicate that the interaction between two 1+ charged ferrocene substituents is capable of causing rotation of the π-stacked entities in acetonitrile solution. The electrostatic repulsion and the forces that induce an eclipsed, π-stacked configuration, however, are of similar energies. If this is the case, the electrostatic repulsion between 2+ and 1+ charges at similar distances with analogous groups in acetonitrile solution is expected to provide a higher population of the un-π-stacked rotamers. This issue is investigated in the next section.

Rotamers formed by stronger repulsive electrostatic forces: To increase the electrostatic repulsion in these ferrocene systems, we have prepared the bipyridyl (bipy) compound **12** [Eq. (3)]. Attempts to incorporate Pd(Cl$_2$) into the bipy ligand using [Pd(CH$_3$CN)$_2$Cl$_2$] failed. The product was a dimer where two PdCl units were bound to a bipy ligand of one ferrocene and the 3-pyridine of the other ferrocene (see Supporting Information for the crystal structure). The ^{1}H NOE cross-peaks are shown in CD$_3$CN at 20°C for **12**. Most of the cross-peaks are unsurprising but the cross-peaks that are seen between *ortho*-protons of the Cp units and the attached pyridine groups (indicated by *) indicate that the
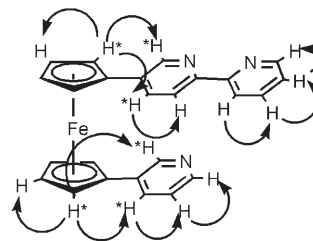
12

pyridine groups are freely rotating about the Cp units. In principle, cross-peaks are expected between the pyridine on one Cp unit and the corresponding pyridine on the other. Despite considerable effort, none was observed between the pyridine groups on different Cp units.

As shown in Equation (4), the 3-pyridine group of **12** can be methylated selectively and this product can form the $PdCl_2$ complex to the bipy group. This product can then be converted to the $Pd(Py)_2$ and $Pd(CH_2C(O)CH_3)(Py)$ salts [Eq. (5)]. In Figures 8–12 are shown the X-ray diffraction crystal structures of systems carrying a variety of charges. All charged crystals are formed as SbF_6^- salts. Table 8 lists
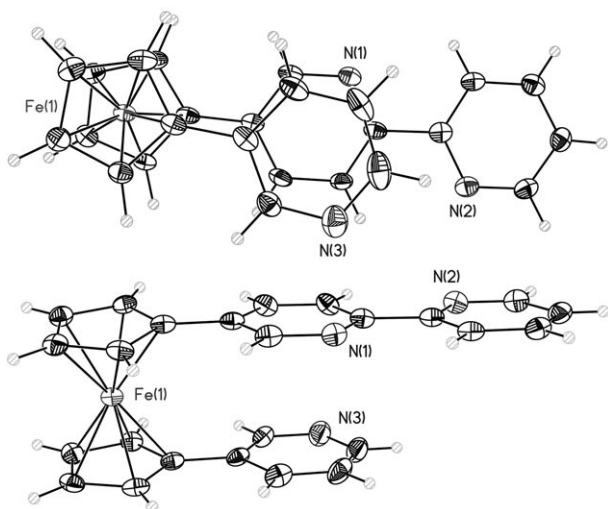

Figure 8. Two perspectives of the solid-state structure of **12**. Thermal ellipsoids are at 50% probability. The hydrogen atoms shown are calculated, they were not located.
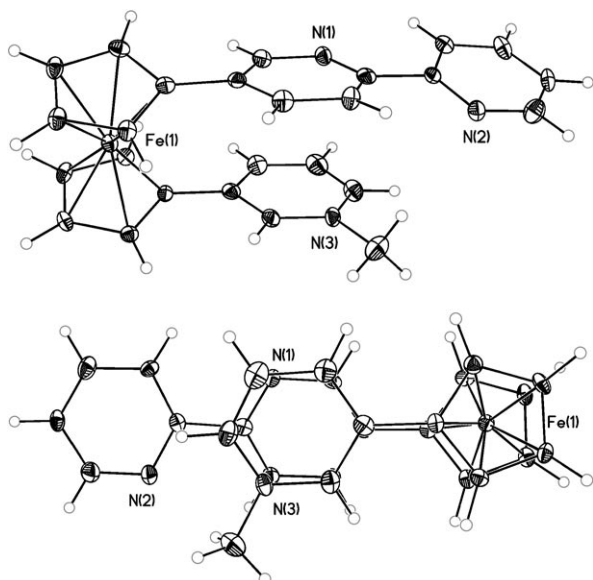

Figure 9. Two perspectives of the solid-state structure of **13** as the SbF_6^- salt. Thermal ellipsoids are at 50% probability. The hydrogen atoms shown are calculated, they were not located. The SbF_6^- ion is omitted for clarity.

Figure 10. Two perspectives of the solid-state structure of **14** as the SbF_6^- salt. Thermal ellipsoids are at 50% probability. The SbF_6^- ion and the hydrogen atoms are omitted for clarity.

the crystallographic data for each of the crystals. Important data related to π-stacking of these complexes are given Table 9.

As can be seen from Figure 8, Figure 9 and Figure 10 and the data in Table 9, the pyridine or pyridinium group is π-stacked on the Cp-bound pyridine of bipy ligand. The two substituents are essentially eclipsed (Cp–Cp angles are small). In all of the cases the nitrogen atom of the pyridine or pyridinium group is *trans* to the corresponding nitrogen of the Cp-bound pyridine group of bipy. The dicationic system **15**, shows small Cp–Cp rotation (17.34°) but considerable π–π overlap remains (see Figure 13 in the Supporting Information). The distance between N(5) and Pd(1) is 6.22 Å. This distance can be compared to that found for the pyridinium N(1) and N(2) distances of the SbF_6^- salts of **7**(H$^+$)$_2$ and **9**; these are 5.66 Å and 6.16 Å, respectively. These similar distances indicate that Coulombic repulsion may be the determining factor in the rotation of the Cp rings, as assumed. It will be noted that for the palladium complex **15**, a distance of 6.22 Å between the metal ion and the pyridinium nitrogen atom will result in more π-overlap between the corresponding pyridine rings than in the cases of **7**(H$^+$)$_2$ and **9**. For the tricationic system, **16**, however, the pyridinium and the dicationic [bipyPd(py)$_2$] units are rotated to almost maximum mutual displacement (Figure 12). The *N*-methylpyridinium groups are disordered in the crystal, with almost equal population of the two shown positions. The Cp carbon atoms attached to the *N*-methylpyridinium group are not resolved for the two positions. It is clearly disordered (Figure 12). The distances between the two positions of the quaternary nitrogen atom and the palladium

Figure 11. Two perspectives of the solid-state structure of **15** as the SbF_6^- salt. Thermal ellipsoids are at 50% probability. The SbF_6^- ions and the hydrogen atoms are omitted for clarity.

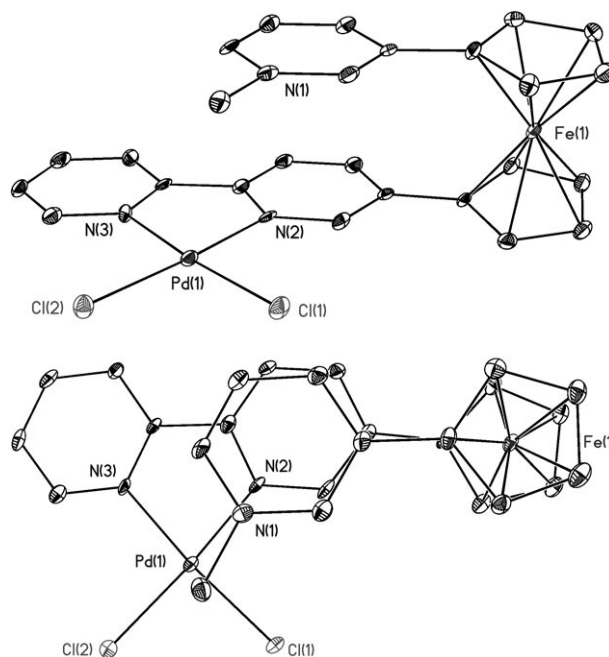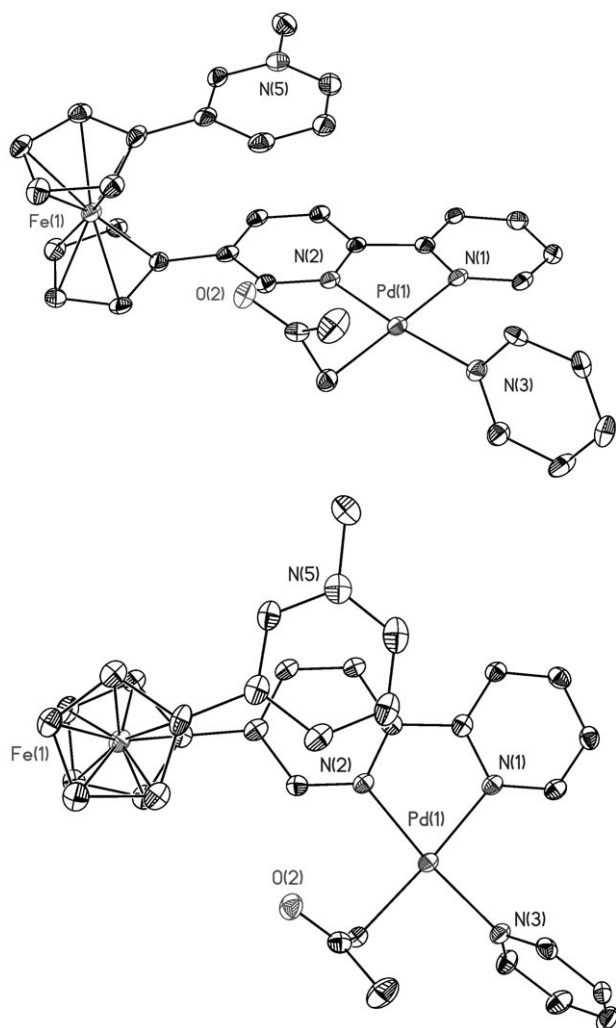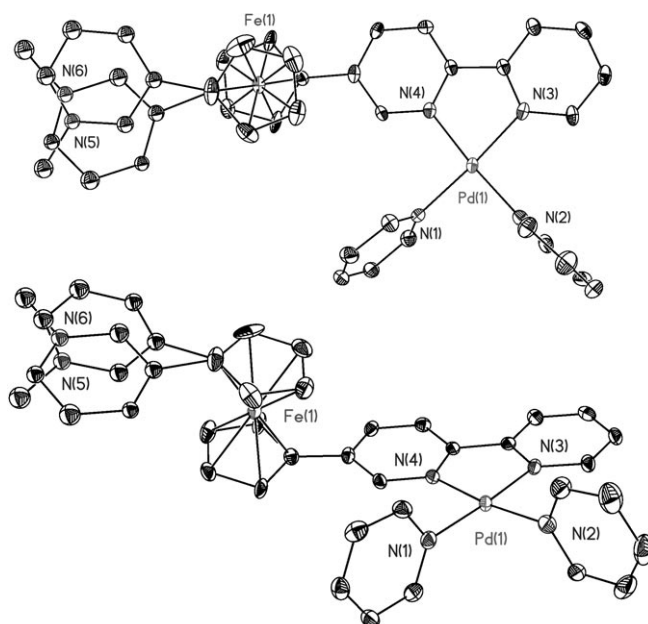

Figure 12. Two perspectives of the solid-state structure of **16** as the SbF_6^- salt. Thermal ellipsoids are at 50% probability. The SbF_6^- ions and the hydrogen atoms are omitted for clarity.

atom are 10.85 and 11.10 Å. This is the first case in which the two groups are fully displaced from each other in the solid state. As noted previously, the crystal structure depends not only on the intramolecular forces but also on the crystal packing interactions. Even so, the structures in the solid state are broadly consistent with chemical shift data in CD_3CN solutions at 27°C (Table 10).
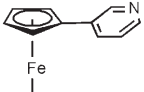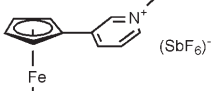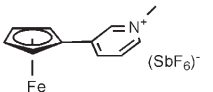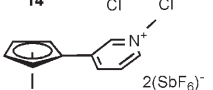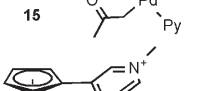
The data in Table 10 indicate that the compounds **12–14** exist in mainly the eclipsed, π-stacked rotameric conformation. The cationic compound **13** appears to have a higher

Table 8. Crystallographic data for **12**, **13**, **14**, **15**, and **16**.

Compound	12	13	14	16	15
formula	$C_{25}H_{19}FeN_3$	$C_{26}H_{22}FeN_3^+ + SbF_6$	$C_{26}H_{22}Cl_2FeN_3Pd + C_2H_3N + SbF_6$	$C_{34}H_{31}FeN_4OPd + C_3H_6O + 2SbF_6$	$C_{36}H_{32}FeN_5Pd + 3SbF_6$
formula weight	834.56	668.07	886.42	1203.46	1397.11
space group	P	$P2_1$	$P\bar{1}$	$P\bar{1}$	$P2_1/c$
a [Å]	9.643(2)	8.117(3)	7.580(2)	8.496(4)	18.949(7)
b [Å]	11525(3)	10.183(4)	10.167(3)	15.244(7)	11.741(4)
c [Å]	17.768(4)	14.664(6)	19.454(6)	16.211(8)	19.635(7)
α [°]	79.162(4)	90.0	90.515(5)	82.548(8)	90.0
β [°]	80.400(4)	101.720(6)	100.723(5)	82.125(8)	101.035(6)
γ [°]	70.768(4)	90.0	98.632(5)	78.219(8)	90.0
V [Å^3]	1819.2(7)	1186.8(8)	1455.3(7)	2024.7(17)	4288(3)
Z	4	2	2	2	4
cryst. size	$0.20\times0.15\times0.04$ mm	$0.20\times0.05\times0.02$ mm	$0.20\times0.10\times0.03$ mm	$0.40\times0.20\times0.03$ mm	$0.25\times0.20\times0.03$ mm
color, habit	red, plate	red, ribbon	red, plate	red-brown, plate	purple, plate
ρ_{calcd} [g cm^{-3}]	1.524	1.869	2.023	1.974	2.164
μ [mm^{-1}]	0.846	1.818	2.275	2.203	2.721
T [K]	100(5)	100(5)	100(5)	100(5)	100(5)
wavelength [Å]	0.71073 (Mo$_{K\alpha}$)	0.71073 (Mo$_{K\alpha}$)	0.71073 (Mo$_{K\alpha}$)	0.71073 (Mo$_{K\alpha}$)	0.71073 (Mo$_{K\alpha}$)
$R(F)$ [%][a]	4.69	4.84	5.11	5.31	7.75
$R(wF^2)$ [%][a]	10.80	7.23	10.31	11.12	19.30

[a] Quantity minimized $= R(wF^2) = \Sigma[w(F_o^2-F_c^2)^2]/\Sigma[(wF_o^2)^2]^{1/2}$; $R = \Sigma\Delta/\Sigma(F_o)$, $\Delta = |(F_o-F_c)|$ $w = 1/[\sigma^2(F_o^2) + (aP)^2 + bP]$, $P = [2F_c^2 + Max(F_o, 0)]/3$.
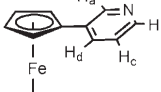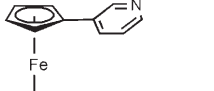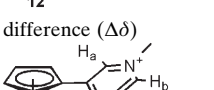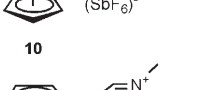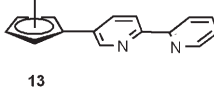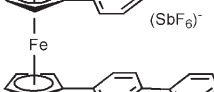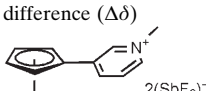
Table 9. Important angles and distances for the crystal structures illustrated in Figures 8–12.

Compound	Cp–Cp [°][a]	Angles Cp–Py [°][b]	Cp–Bipy [°][b]	Distance Py–Py [Å][c]
12	2.71	5.10	9.00	3.39
13	1.44	17.30	24.50	3.26
14	7.43	8.30	11.10	3.29
15	17.34	11.90	8.80	3.24
16	159.64 −160.39	5.90 5.90	16.60	–

[a] Cp-Cp rotation angle; eclipsed angle is 0°. [b] Interplanar angle between Cp and pyridine (or pyridinium), py, and the Cp attached pyridine of bipy, Cp-bipy. [c] Average interplanar separation between the pyridines on the different Cp units.

population of the eclipsed, π-stacked form than the neutral compound **12**, an observation that supports the assertion that the π–π stacking is more effective for charged–neutral than for neutral–neutral aromatic pairs of molecules. The proton chemical shift differences of **14** are different from those observed for **12** and **13**, in that **14** has only a small upfield shift for the H_a and H_b protons. The H_c and H_d protons of **14**, on the other hand, show substantial upfield shifts. These observations suggest that the favored π-stacked conformation for **12** and **13** has all four protons (H_a to H_d) roughly equally disposed over the requisite pyridine group of bipy, whereas **14** has the pyridinium group displaced such that H_c and H_d lie over the requisite pyridine of the bipyPdCl$_2$ and that the corresponding H_a and H_b are not aligned over the π-cloud of the same pyridine. The dicationic complex **15** shows chemical shifts of its pyridinium pro-

Table 10. Chemical shifts of the protons of the pyridine or N-methylpyridinium substituent for the compounds **12** to **16** in [D$_3$]acetonitrile solution.

Compound	Chemical Shift (δ) H_a	H_b	H_c	H_d
8	8.73	8.38	7.24	7.86
12	8.48	8.08	6.90	7.60
difference (Δδ)	−0.25	−0.30	−0.34	−0.26
10	8.63	8.45	7.83	8.34
13	8.13	8.06	7.36	7.87
difference (Δδ)	−0.50	−0.39	−0.48	−0.47
14	8.55	8.39	7.46	7.83
difference (Δδ)	−0.08	−0.06	−0.37	−0.51
15	8.54	8.37	7.66	8.08
difference (Δδ)	−0.08	−0.08	−0.17	−0.26
16	8.55	8.36	7.81	8.24
difference (Δδ)	−0.08	−0.09	−0.02	−0.10

tons which suggest that the major rotameric conformation is a structure that has the two groups rotated but some overlap remains for the H_c and H_d protons. For the tricationic

system, ^{1}H NMR chemical shifts indicate the least amount of π-stacking in solution, as expected from the electrostatic considerations and from the results of X-ray diffraction.

Reversibility: The diprotonated compound **7**(H^{+})₂ and the monoprotonated system **11**(H^{+}), revert to their original rotameric conformations when the protons are neutralized by addition of triethylamine to acetonitrile solutions. Similarly, the dipyridine palladium complex **16** is converted cleanly to the dichloro analogue **14**, upon addition of two equivalents of tetra-*n*-butylammonium chloride in acetonitrile solution. Thus in both cases these electrostatic drivers are cleanly reversible, a condition necessary for the development of molecular motors.

Discussion

This study of the potential of using substituted ferrocenes as protonmotive drivers for developing molecular motors and machines has shown that it may be possible to use them for this purpose. It is clear, however, that in solvents of high dielectric constant, such as acetonitrile, the amount of torque generated by electrostatic repulsion by the dicationic systems is insufficient to drive the two substituents away from populations where some π-overlap occurs. For the tricationic driver **16**, however, sufficient torque is present to essentially uncouple the two substituents.

This report has not investigated in detail one other complicating factor in developing these electrostatic drivers. As the dielectric constant of the medium is decreased, the electrostatic interaction will be increased but the tendency for ion-pairing will also increase. These two phenomena are likely to act in opposition to each other and lead to diminution of the electrostatic repulsion that is gained in solvents of low dielectric constant.

Overall, the results observed in solution are consistent with those observed in the solid state, despite the possible effects of crystal packing on the solid-state structures. As noted earlier and as is shown in Figure 1 and Figure 2, the approximate electrostatic calculations indicate that the Coulombic interactions for a pair of 1+ substituents are similar to the stabilizing interactions that lead to the eclipsed conformation of the Cp rings and of the two substituents. The results presented here are consistent with these conclusions. Inspection of Table 1, Table 2, and Table 4 and the structures shown in Figure 4 and Figure 5 indicate the most populated rotamers of the di-1+ systems are those where some overlap between the two pyridine substituents remains. The data in Table 5 and Table 7 and the structures shown in Figure 6 and Figure 7 indicate that the greater π–π interaction (than for the dipyridine systems) between the two substituents is nearly sufficient to overcome the electrostatic repulsion. Consistently, as illustrated by the structures in Figures 10–12 and by the ^{1}H NMR spectral data in Table 10 the two substituents can be completely separated when a 2+ with 1+ interaction obtains (Figure 12) but for a similar

system (Figure 11) when a pair of 1+ charges is involved the most populated rotamer is one where considerable π–π interaction remains. It is perhaps surprising that electrostatic repulsions between ferrocene substituents are of a similar magnitude to the attractive interactions between π-substituents. Probably the high dielectric constant of acetonitrile attenuates the Coulombic repulsion as the two charges separate.

During the reviewing time of this article, two reports on the use of ferrocenes as rotary motors have appeared. One of these involved a gas-phase study of the preferred rotameric conformation of the ferrocene carboxylates [Fe-(C₅H₄CO₂^{-})₂][2-] and [Fe(C₅H₄CO₂^{-})(C₅H₄CO₂H)][-]. It was shown[27] that the conformation of the dicarboxylate was where the two carboxylate groups were rotated away from each other. The other report,[28] concerned the use of ferrocene rotation for inducing concerted rotation about a distant single bond when the ferrocene rings were caused to rotate by photochemical isomerization of diazo groups. These two examples demonstrate that the ferrocene group is likely to find increasing use in the design of rotary motors.

The data presented here serve to indicate the approximate amount of protonmotive torque that can be generated by these electrostatic drivers and are a prerequisite for developing the ferrocene platform for the construction of molecular motors.

Experimental Section

General procedures: All reagents were obtained from commercial suppliers and were used without further purification. All reactions were performed under an atmosphere of argon, unless otherwise specified. ^{1}H and ^{13}C NMR spectra were recorded using a Bruker DRX500 or a Bruker DMX500 Fourier transform spectrometer. Proton and carbon chemical shifts, δ, are reported in ppm, and referenced to tetramethylsilane (TMS). Coupling constants, *J*, are reported in hertz. Electronic absorption spectra were obtained by using a Perkin Elmer Lambda 6 UV/Vis spectrophotometer. For studying protonation of substrates at a given wavelength and acid concentration, the absolute change in absorbance, ($|\Delta A|$), was calculated by subtracting the acid dependent absorbance from the absorbance in the absence of acid, ($|\Delta A|_o$). The absolute change in chemical shift, ($|\Delta\delta|$) is calculated similarly. Elemental analyses were performed by Desert Analytics, Tucson, Arizona. Conductance measurements were performed at 23°C with 1×10^{-3} M samples using an YSI Scientific model 35 conductance meter. Acetonitrile was dried over CaH₂, tetrahydrofuran (THF) was dried over potassium/benzophenone ketyl, diethyl ether was dried over sodium/benzophenone ketyl, and methylene chloride was dried over CaH₂. Dry trifluoroacetic acid (TFA) was obtained by distillation from a solution containing 5% trifluoroacetic anhydride. Thin-layer chromatography was carried out using precoated silica gel (Whatman PE SIL G/UV) or precoated aluminum oxide (J. T. Baker, aluminum oxide IB-F). Silica gel 60 Å (Merck, 230–400 mesh) and aluminum oxide 58 Å (either activated, basic, Brockman I or activated, neutral, Brockman I) were used for chromatography as indicated. Celite is J. T. Baker Celite 503. Ferrocene-1,1′-diboronic acid,[21] 5-bromo-2,2′-bipyridine[29] were prepared by literature methods. Ferroceneboronic acid,[30] graphite, and hexafluoroantimonic acid hexahydrate (HSbF₆·6H₂O) were obtained from the Aldrich Chemical Co. and used as received.

[3-Pyridylferrocene] (8): A 100-mL flask was charged with 3-bromopyridine (1.00 g, 6.32 mmol) dissolved in a mixture of dioxane (10 mL) and

1 M aqueous Na_2CO_3 (10 mL). The catalyst $PdCl_2[1,1'$-bis(diphenylphosphino)ferrocene] (0.250 g, 0.34 mmol) was added to the reaction mixture followed by a mixture of ferroceneboronic acid (0.85 g, 3.69 mmol) and 3 M aqueous NaOH (3 mL) in DME (10 mL). The reaction mixture was refluxed for 24 h. At the end of this period the reaction mixture was stirred until it had cooled to room temperature and was then poured into ice-water (200 mL). The resulting mixture was extracted with ethyl acetate (3×100 mL). The organic layer was washed with NH_4Cl solution (100 mL), water (100 mL), and brine (100 mL). The resulting orange solution was dried with Na_2SO_4 and concentrated to an orange-red solid. The solid residue was dissolved in CH_2Cl_2 and chromatographed on basic alumina with CH_2Cl_2/hexanes (50:50). The eluted solvent was removed under reduced pressure to yield an orange powder, which was recrystallized by vapor diffusion of CH_2Cl_2 solution with hexanes. The orange needles (0.63 g, 55%) were collected by filtration and were washed with cold hexanes and vacuum-dried. ^1H NMR (CD_3CN, 27°C, 500 MHz): $\delta =$ 4.04 (s, 5H), 4.37 (t, $^1J = 1.8$ Hz, 2H), 4.81 (t, $^1J = 1.8$ Hz, 2H), 7.26 (m, 1H), 7.88 (m, 1H), 8.41 (dd, $^1J = 4.7$ Hz, $J_2 = 1.5$ Hz, 1H), 8.80 ppm (s, 1H); ESI-MS (MeOH): m/z: 263 [M], 264 [$M+1$]; conductivity: Λ_M-(CH_3CN) $= 0.84$ Ω^{-1} cm^2 mol^{-1}.

[N-Methyl-3-pyridylferrocene](SbF$_6$) (10): A 10-mL flask was charged with **8** (0.130 g, 0.49 mmol) dissolved in CH_2Cl_2 (2 mL). CH_3I (0.69 g, 0.30 mL, 4.94 mmol) was added to the orange solution and the reaction mixture was stirred at room temperature for 16 h, during which time a red precipitate formed. The precipitate was isolated by filtration and was washed with cold CH_2Cl_2, Et_2O and pentane. The red iodo salt (0.200 g) was dissolved in acetone (3 mL) and AgSbF$_6$ (0.170 g, 0.49 mmol) was added as a solid to the red solution. A precipitate formed immediately and the mixture was stirred at room temperature for 30 min. The orange suspension was filtered through celite and the solvent was removed under reduced pressure. The solid orange residue was dissolved into CH_2Cl_2 and vapor diffused with hexanes. Orange needles were obtained. They were collected and were washed with cold hexanes and vacuum-dried (0.220 g, 95%). ^1H NMR (CD_3CN, 27°C, 500 MHz): $\delta = 4.15$ (s, 5H), 4.25 (s, 3H), 4.60 (t, $^1J = 1.8$ Hz, 2H), 4.90 (t, $^1J = 1.9$ Hz, 2H), 7.82 (m, 1H), 8.34 (d, $^1J = 5.9$ Hz, 1H), 8.45 (d, $^1J = 8.2$ Hz, 1H), 8.63 ppm (s, 1H); ESI-MS (CH_3CN): m/z 278 [M−SbF$_6$]; conductivity: Λ_M(CH_3CN) $= 124$ Ω^{-1} cm^2 mol^{-1}; elemental analysis calcd (%) for $C_{16}H_{16}F_6FeNSb$: C 37.39, H 3.14, N 2.73; found: C 37.71, H 2.98, N 2.35.

[1,1′-(3-Pyridyl)ferrocene] (7): In 250-mL flask 3-bromopyridine (3.00 g, 18.98 mmol) was dissolved in a mixture of dioxane (50 mL) and 1 M aqueous Na_2CO_3 (40 mL). The catalyst [PdCl$_2$(1,1′-bis(diphenylphosphino)ferrocene)] (0.60 g, 0.82 mmol) was added to the reaction mixture followed by a mixture of ferrocene-1,1′-diboronic acid (2.00 g, 7.31 mmol) and 3 M aqueous NaOH (5 mL) in DME (35 mL). The reaction mixture was refluxed for 24 h. At the end of this time, the reaction mixture was stirred until it had cooled to room temperature and was then poured into ice-water (250 mL). The resulting mixture was extracted with ethyl acetate (3×100 mL). The organic layer was washed with NH_4Cl solution (100 mL), water (100 mL), and Brine (100 mL). The resulting orange solution was dried over Na_2SO_4 and was concentrated to an orange-red solid. The solid residue was dissolved into CH_2Cl_2 and was chromatographed on silica gel with CH_2Cl_2/MeOH (98:2). The eluted solvent was removed under reduced pressure yielding an orange powder, which was recrystallized by vapor diffusion of CH_2Cl_2 solution with hexanes. The orange needles (1.68 g, 68%) were collected by filtration and were washed with cold hexanes and were vacuum-dried. ^1H NMR ([D$_6$]acetone, 27°C, 500 MHz): $\delta = 4.34$ (t, $^1J = 1.86$ Hz, 4H), 4.75 (t, $^1J = 1.88$ Hz, 4H), 7.06 (m, 2H), 7.58 (m, 2H), 8.31 (dd, $^1J = 4.7$ Hz, $^2J = 1.5$ Hz, 2H), 8.54 ppm (d, $^1J = 1.8$ Hz, 2H); ESI-MS (MeOH): m/z: 340 [M], 341 [$M+1$]; conductivity: Λ_M(CH_3CN) $= 0.59$ Ω^{-1} cm^2 mol^{-1}; elemental analysis calcd (%) for $C_{20}H_{16}FeN_2$: C 70.61, H 4.74, N 8.23; found: C 70.72, H 5.01, N 8.18.

[1,1′-(N-Methyl-3-pyridyl)ferrocene](SbF$_6$)$_2$ (9): A 10-mL flask was charged with **7** (0.100 g, 0.29 mmol) dissolved in CH_2Cl_2 (2 mL). CH_3I (0.417 g, 0.18 mL, 2.95 mmol) was added to the orange solution and the reaction mixture was stirred at room temperature for 16 h, during which time a deep red precipitate formed. The precipitate was isolated by filtra-

tion and was washed with cold CH_2Cl_2, Et_2O, and pentane. The red iodo salt (0.170 g) was dissolved in acetone (3 mL) and AgSbF$_6$ (0.188 g, 0.55 mmol) was added as a solid to the red solution. AgI precipitated immediately and the mixture was stirred at room temperature for 30 min. The resulting red suspension was filtered through celite and the solvent was removed under reduced pressure. The solid red residue was dissolved into CH_2Cl_2 and was vapor-diffused with hexanes. Red blocks formed and were filtered and were washed with cold hexanes and vacuum-dried (0.185 g, 75%). ^1H NMR (CD_3CN, 27°C, 500 MHz): $\delta = 4.25$ (s, 6H), 4.56 (sb, 4H), 4.90 (sb, 4H), 7.76 (m, 2H), 8.24 (d, $^1J = 8.0$ Hz, 2H), 8.38 (d, $^1J = 5.6$ Hz, 1H), 8.55 ppm (s, 1H); conductivity: Λ_M(CH_3CN) $= 259$ Ω^{-1} cm^2 mol^{-1}; ESI-MS (CH_3CN): m/z 606 [M−SbF$_6$]; elemental analysis calcd (%) for $C_{22}H_{22}F_{12}FeN_2Sb_2$: C 31.39, H 2.63, N 3.33; found: C 31.34, H 2.55, N 3.03.

3-Bromo-8-nitroquinoline and 3-bromo-5-nitroquinoline: To a solution of 3-bromoquinoline (10.0 g, 48.0 mmol) in concentrated H_2SO_4 (20 mL) cooled in a water/ice bath was added dropwise 16 mL of a concentrated H_2SO_4/concentrated HNO$_3$ mixture (6:2). The reaction mixture was maintained at low temperature, stirred rapidly, and monitored by thin-layer chromatography until all of the 3-bromoquinoline had been consumed (ca. 3 h). The mixture was diluted with water (50 mL) and NaOH added until the solution reached pH 10–11. The resulting solution was extracted with diethyl ether (2×50 mL), the organic phase dried over anhydrous magnesium sulfate, and the solvent was removed under reduced pressure to give an ≈ 8:2 mixture of 3-bromo-5-nitroquinoline and 3-bromo-8-nitroquinoline, respectively. Crystallization of this mixture from ethyl acetate afforded 3-bromo-5-nitroquinoline (8.8 g, 72%). ^1H NMR ($CDCl_3$): $\delta = 9.26$ (dd, $^1J = 2.1$ Hz, $^2J = 0.7$ Hz, 1H), 9.04 (d, $^1J = 6.4$ Hz, 1H), 8.44 (m, 2H), 7.86 ppm (t, $^1J = 8.1$ Hz, 1H); ESI-MS (MeOH): m/z: 253 [M], 254 [$M+1$]; elemental analysis calcd (%) for $C_9H_5BrN_2O_2$: C 42.72, H 1.99, N 11.07; found: C 42.59, H 2.15, N 11.28.

The solvent was removed from the mother liquor to yield an off-white residue which contains both 3-bromo-8-nitroquinoline and 3-bromo-5-nitroquinoline. This residue was recrystallized twice from boiling cyclohexanes to yield the desired 3-bromo-8-nitroquinoline (2.05 g, 17%). ^1H NMR ($CDCl_3$): $\delta = 9.05$ (d, $^1J = 2.1$ Hz, 1H), 8.43 (d, $^1J = 2.1$ Hz, 1H), 8.05 (d, $^1J = 7.4$ Hz, 1H), 7.96 (d, $^1J = 8.1$ Hz, 1H), 7.66 ppm (t, $^1J = 7.8$ Hz, 1H); ESI-MS (MeOH): m/z: 253 [M], 254 [$M+1$]; elemental analysis calcd (%) for $C_9H_5BrN_2O_2$: C 42.72, H 1.99, N 11.07; found: C 42.76, H 2.01, N 10.98.

[1-(3-Pyridyl)-1′-(boronic acid)ferrocene] (18): Into a 100-mL flask was added 3-bromopyridine (1.16 g, 7.31 mmol) dissolved in a mixture of dioxane (10 mL) and 1 M aqueous Na_2CO_3 (10 mL). The catalyst [PdCl$_2$-(1,1′-bis(diphenylphosphino)ferrocene)] (0.60 g, 0.82 mmol) was added to the reaction mixture followed by a mixture of ferrocene-1,1′-diboronic acid (2.00 g, 7.31 mmol) and 3 M aqueous NaOH (3 mL) in DME (10 mL). The reaction mixture was refluxed for 12 min (5 min ramp, 7 min hold) in a CEM microwave reactor (power 150 W). At the end of this period the reaction mixture was stirred until it had cooled to room temperature and was then poured into ice-water (200 mL). The resulting mixture was extracted with ethyl acetate (3×100 mL). The organic layer was washed with NH_4Cl solution (100 mL), water (100 mL), and brine (100 mL). The resulting orange solution was dried with Na_2SO_4 and was concentrated to an orange-red solid. The solid residue was dissolved into acetone and chromatographed on silica gel with acetone as the eluant. The eluted solvent was removed under reduced pressure yielding an orange powder, which was slurried in hexanes, sonicated, then filtered. The orange powder (1.36 g, 62%) was washed with cold hexanes and vacuum-dried. ^1H NMR ([D$_6$]acetone, 27°C, 500 MHz): $\delta = 4.20$ (t, $^1J = 1.81$ Hz, 2H), 4.34 (t, $^1J = 1.90$ Hz, 2H), 4.36 (t, $^1J = 1.82$ Hz, 2H), 4.74 (t, $^1J = 1.91$ Hz, 2H), 6.71 (sb, 2H), 7.24 (m, 1H), 7.90 (m, 1H), 8.36 (d, $^1J = 4.64$ Hz, 1H), 8.73 ppm (s, 1H); ESI-MS (MeOH): m/z 306 [M], 307 [$M+1$], 336 [$M+2$MeOH-2H$_2$O]; elemental analysis calcd (%) for $C_{15}H_{14}BFeNO_2$: C 58.70, H 4.60, N 4.56; found: C 60.25, H 4.70, N 4.45.

[1-(3-Pyridyl)-1′-(3-(8-nitroquinoline)ferrocene] (19): Into a 50-mL flask was added 3-bromo-8-nitroquinoline (1.00 g, 3.95 mmol) dissolved in a mixture of dioxane (10 mL) and 1 M aqueous Na_2CO_3 (10 mL). The catalyst [PdCl$_2$(1,1′-bis(diphenylphosphino)ferrocene)] (0.40 g, 0.54 mmol)

was added to the reaction mixture followed by a mixture of **18** (1.00 g, 3.26 mmol) and 3 M aqueous NaOH (3 mL) in DME (10 mL). The reaction mixture was refluxed for 24 h. At the end of this period the reaction mixture was stirred until it had cooled to room temperature and was then poured into ice-water (100 mL). The resulting mixture was extracted with ethyl acetate (3×100 mL). The organic layer was washed with NH$_4$Cl solution (100 mL), water (100 mL), and brine (100 mL). The resulting orange solution was dried with Na$_2$SO$_4$ and concentrated to an orange-red solid. The solid residue was dissolved into CH$_2$Cl$_2$ and chromatographed on silica gel with CH$_2$Cl$_2$/THF (90:10). The eluted solvent was removed under reduced pressure yielding a red-orange powder, which was recrystallized by vapor diffusion of an acetone solution with hexanes. The red-orange needles (0.75 g, 53%) were collected by filtration and were washed with cold hexanes and were vacuum dried. ^{1}H NMR ([D$_6$]acetone, 27°C, 500 MHz): $\delta = 4.43$ (t, $^1J = 1.9$ Hz, 2H), 4.51 (t, $^1J = 1.9$ Hz, 2H), 4.86 (t, $^1J = 1.9$ Hz, 2H), 5.02 (t, $^1J = 1.9$ Hz, 2H), 6.64 (m, 1H), 7.35 (m, 1H), 7.69 (t, $^1J = 7.4$ Hz, 1H), 7.84 (dd, $^1J = 4.8$ Hz, $^2J = 1.6$ Hz, 1H), 7.94 (dd, $^1J = 8.2$ Hz, $^2J = 1.3$ Hz, 1H), 8.01–8.03 (m, 1H), 8.05 (d, $^1J = 2.3$ Hz, 2H), 8.41 (m, 1H), 8.91 ppm (d, $^1J = 2.1$ Hz, 1H); ESI-MS (MeOH): m/z 435 [M], 436 [M+1]; elemental analysis calcd (%) for C$_{24}$H$_{17}$FeN$_3$O$_2$: C 66.23, H 3.94, N 9.65; found: C 66.50, H 4.31, N 9.46.

[1-(*N*-Methyl-3-pyridyl)-1′-(3-(8-nitroquinoline)ferrocene](SbF$_6$) (20): A 10-mL flask was charged with **19** (0.150 g, 0.34 mmol) dissolved in CH$_2$Cl$_2$ (3 mL). CH$_3$I (0.520 g, 3.68 mmol) was added to the red solution and the reaction mixture was stirred at room temperature for 16 h, during which time a deep red precipitate formed. The precipitate was isolated by filtration and was washed with cold CH$_2$Cl$_2$, Et$_2$O, and pentane. The deep red iodo salt (0.191 g) was dissolved in acetone (5 mL) and AgSbF$_6$ (0.114 g, 0.33 mmol) was added as a solid to the red solution. AgI precipitated immediately and the mixture was stirred a room temperature for 30 min. The reaction mixture was filtered through celite and the solvent removed under reduced pressure. The solid red residue was dissolved into acetone and was vapor-diffused with hexanes. The red blocks so obtained were collected by filtration and then were washed with cold hexanes and vacuum-dried (0.185 g, 78%). ^{1}H NMR (CD$_3$CN, 27°C, 500 MHz): $\delta = 3.92$ (s, 3H), 4.59 (sb, 2H), 4.65 (sb, 2H), 4.88 (sb, 2H), 5.04 (sb, 2H), 7.00 (m, 1H), 7.70 (d, $^1J = 7.8$ Hz, 1H), 7.75 (m, 1H), 7.77 (d, $^1J = 8.1$ Hz, 1H), 7.98 (d, $^1J = 8.1$ Hz, 1H), 8.02 (d, $^1J = 7.4$ Hz, 1H), 8.05 (d, $^1J = 2.0$ Hz, 1H), 8.14 (s, 1H), 8.65 ppm (d, $^1J = 2.0$ Hz, 1H); conductivity: Λ_M(CH$_3$CN) = 137 Ω^{-1}cm^{2}mol^{-1}; ESI-MS (CH$_3$CN): m/z: 450 [M−SbF$_6$]; elemental analysis calcd (%) for C$_{25}$H$_{20}$F$_6$FeN$_3$O$_2$: C 43.77, H 2.94, N 6.13; found: C 44.00, H 2.98, N 6.21.

[1-(*N*-Methyl-3-pyridyl)-1′-(3-(8-aminoquinoline)ferrocene](SbF$_6$) (11): A 10-mL flask was charged with **20** (0.100 g, 0.14 mmol) dissolved in CH$_3$CN (3 mL) and EtOH (3 mL). N$_2$H$_4$·H$_2$O (0.020 g. 0.020 mL, 0.39 mmol) and graphite (0.500 g) were added to the red solution and the reaction mixture was heated at reflux for 36 h. The reaction mixture was filtered through celite and the solvent was removed under reduced pressure. The deep red residue was slurried in hexanes and was filtered. The solid red residue was dissolved into CH$_2$Cl$_2$ and was vapor-diffused with hexanes. The red blocks so obtained were collected by filtration and were washed with cold hexanes and were vacuum-dried (0.080 g, 82%). ^{1}H NMR (CD$_3$CN, 27°C, 500 MHz): $\delta = 3.77$ (s, 3H), 4.48 (t, $J_1 = 1.7$ Hz, 2H), 4.59 (t, $^1J = 1.7$ Hz, 2H), 4.82 (t, $^1J = 1.7$ Hz, 2H), 4.96 (t, $^1J = 1.7$ Hz, 2H), 5.27 (sb, 2H), 6.88–6.90 (m, 2H), 6.95–6.97 (m, 1H), 7.33 (t, $^1J = 7.8$ Hz, 1H), 7.44 (d, $^1J = 5.7$ Hz, 1H), 7.62 (d, $^1J = 2.1$ Hz, 1H), 7.89 (sb, 1H), 8.40 ppm (d, $J_1 = 2.3$, 1H); conductivity: Λ_M(CH$_3$CN) = 122 Ω^{-1}cm^{2}mol^{-1}; ESI-MS (CH$_3$CN): m/z: 420 [M−SbF$_6$]$^+$; elemental analysis calcd (%) for C$_{25}$H$_{22}$F$_6$FeN$_3$Sb: C 45.77, H 3.38, N 6.40; found: C 45.65, H 3.54, N 6.69.

[1-(3-Pyridyl)-1′-(5-2,2′-dipyridyl)ferrocene] (12): A 50-mL flask was charged with 5-bromo-2,2′-bipyridine (1.25 g, 5.31 mmol) dissolved in a mixture of dioxane (10 mL) and 1 M aqueous Na$_2$CO$_3$ (10 mL). The catalyst [PdCl$_2$(1,1′-bis(diphenylphosphino)ferrocene)] (0.40 g, 0.54 mmol) was added to the reaction mixture followed by a solution of **18** (0.80 g, 2.60 mmol) in 3 M aqueous NaOH (3 mL) in DME (10 mL). The reaction mixture was refluxed for 24 h. At the end of this period the reaction mix-

ture was stirred until it had cooled to room temperature and was then poured into ice-water (100 mL). The resulting mixture was extracted with ethyl acetate (3×100 mL). The organic layer was washed with NH$_4$Cl solution (100 mL), water (100 mL), and brine (100 mL). The resulting orange solution was dried over Na$_2$SO$_4$ and was concentrated to an orange-red solid. The solid residue was dissolved into CH$_2$Cl$_2$ and was chromatographed on silica gel with CH$_2$Cl$_2$/acetone (90:10). The eluted solvent was removed under reduced pressure yielding orange powder, which was recrystallized by vapor-diffusion of an acetone solution with hexanes. The orange needles (0.75 g, 70%) were collected by filtration and were washed with cold hexanes and were vacuum dried. ^{1}H NMR ([D$_6$]acetone, 27°C, 500 MHz): $\delta = 4.38$ (t, $^1J = 1.8$ Hz, 2H), 4.40 (t, $^1J = 1.8$ Hz, 2H), 4.80 (t, $^1J = 1.8$ Hz, 2H), 4.84 (t, $^1J = 1.8$ Hz, 2H), 6.96 (m, 1H), 7.39 (m, 1H), 7.58 (m, 1H), 7.70 (dd, $^1J = 8.2$ Hz, $^2J = 2.3$ Hz, 1H), 7.91 (m, 1H), 8.18 (m, 2H), 8.44 (d, $^1J = 7.9$ Hz, 1H), 8.55 (d, $^1J = 1.6$ Hz, 1H), 8.59 (d, $^1J = 2.1$ Hz, 1H), 8.67 ppm (m, 1H); ESI-MS (MeOH): m/z: 417 [M], 418 [M+1]; elemental analysis calcd (%) for C$_{25}$H$_{19}$FeN$_3$: C 71.96, H 4.59, N 10.07; found: C 72.08, H 4.69, N 9.98.

[1-(*N*-Methyl-3-pyridyl)-1′-(5-2,2′-dipyridyl)ferrocene](SbF$_6$) (13): A 10-mL flask was charged with **12** (0.150 g, 0.35 mmol) dissolved in CH$_2$Cl$_2$ (2 mL). CH$_3$I (0.507 g, 3.59 mmol) was added to the orange solution and the reaction mixture was stirred at room temperature for 16 h, during which time a deep red precipitate formed. The precipitate was isolated by filtration and was washed with cold CH$_2$Cl$_2$, Et$_2$O, and pentane. The deep red iodo salt (0.200 g) was dissolved in acetone (5 mL) and AgSbF$_6$ (0.122 g, 0.35 mmol) was added as a solid to the red solution. AgI precipitated immediately and the mixture was stirred at room temperature for 30 min. The reaction mixture was filtered through celite and the solvent was removed under reduced pressure. The solid red residue was dissolved into CH$_2$Cl$_2$ and was vapor-diffused with hexanes. The red needles so obtained were filtered and were washed with cold hexanes and vacuum-dried (0.220 g, 90%). ^{1}H NMR (CD$_3$CN, 27°C, 500 MHz): $\delta = 4.01$ (s, 3H), 4.51 (t, $^1J = 1.8$ Hz, 2H), 4.63 (t, $^1J = 1.8$ Hz, 2H), 4.87 (t, $^1J = 1.8$ Hz, 2H), 4.92 (t, $^1J = 1.8$ Hz, 2H), 7.35 (m, 1H), 7.45 (m, 1H), 7.55 (m, 1H), 7.87 (d, $^1J = 5.9$ Hz, 1H), 7.95 (m, 1H), 7.97 (d, $^1J = 8.2$ Hz, 1H), 8.05 (d, $^1J = 8.2$ Hz, 1H), 8.13 (s, 1H), 8.55 (m, 2H), 8.70 ppm (m, 1H); conductivity: Λ_M(CH$_3$CN) = 137 Ω^{-1}cm^{2}mol^{-1}; ESI-MS (CH$_3$CN): m/z: 432 [M−SbF$_6$]; elemental analysis calcd (%) for C$_{26}$H$_{22}$F$_6$FeN$_3$Sb: C 46.74, H 3.32, N 6.29; found: C 46.29, H 3.50, N 5.84.

[1-(*N*-Methyl-3-pyridyl)-1′-(5-2,2′-dipyridyl)ferrocenePdCl$_2$] (14): A 25-mL flask was charged with **13** (0.130 g, 0.19 mmol) dissolved in acetone (8 mL). [Pd(NCCH$_3$)$_2$Cl$_2$] (0.051 g, 0.19 mmol) was added as a solid to the red solution. The reaction mixture was stirred at room temperature for 1 h, during which time a purple solid formed. The solid was isolated by filtration and was washed with Et$_2$O and pentane. The purple residue was dissolved into CH$_3$CN and was vapor-diffused with Et$_2$O. The purple needles so obtained were collected by filtration and were washed with cold hexanes and were vacuum-dried (0.160 g, 97%). ^{1}H NMR (CD$_3$CN, 27°C, 500 MHz): $\delta = 4.46$ (s, 3H), 4.62 (m, 4H), 4.90 (m, 4H), 7.45 (m, 1H), 7.68 (m, 1H), 7.81 (d, $^1J = 8.2$ Hz, 1H), 8.01 (d, $^1J = 8.4$ Hz, 1H), 8.06 (m, 1H), 8.17 (d, $^1J = 8.1$ Hz, 1H), 8.22 (m, 1H), 8.39 (d, $^1J = 5.9$ Hz, 1H), 8.55 (s, 1H), 8.70 (d, $^1J = 2.2$ Hz, 1H), 9.22 ppm (m, 1H); conductivity: Λ_M(CH$_3$CN) = 126 Ω^{-1}cm^{2}mol^{-1}; ESI-MS (CH$_3$CN): m/z: 610 [M−SbF$_6$]; elemental analysis calcd (%) for C$_{26}$H$_{22}$Cl$_2$F$_6$FeN$_3$PdSb: C 36.94, H 2.62, N 4.97; found: C 36.61, H 2.71, N 4.65.

[1-(*N*-Methyl-3-pyridyl)-1′-(5–2,2′-dipyridyl)ferrocenePd(Py)$_2$](SbF$_6$)$_3$ (15 and 16): A 25-mL flask was charged with **14** (0.100 g, 0.11 mmol) dissolved in acetone (8 mL). AgSbF$_6$ (0.085 g, 0.24 mmol) was added as a solid to the purple solution. The reaction mixture was stirred at room temperature for 1 h, during which time AgCl precipitated. The AgCl was removed by Schlenk filtration. Pyridine (0.22 g, 0.26 mmol) was added to the solution and the reaction mixture was stirred at room temperature for 1 h. The solvent volume was reduced to half of the initial amount and the purple acetone solution was vapor-diffused with Et$_2$O. A mixture of purple and red/brown crystals was obtained during the crystallization from acetone/Et$_2$O. These crystals were separated by hand under a microscope. Yield: The dark purple crystals of **16** (0.126 g, 75%). Red-brown crystals of **15** (0.020 g, 15%). Compound **16** alone can be generat-

ed without the formation of **15**, in an analogous procedure to above by using acetontrile (8 mL) as the solvent.

16 ^{1}H NMR (CD$_3$CN, 27 °C, 500 MHz): $\delta = 4.27$ (s, 3H), 4.37 (sb, 2H), 4.43 (sb, 2H), 4.51 (sb, 2H), 4.83 (sb, 2H), 7.00 (s, 1H), 7.35 (d, $^1J = 5.3$ Hz, 1H), 7.57 (t, $^1J = 4.8$ Hz, 1H), 7.75 (t, $^1J = 6.3$ Hz, 2H), 7.81 (t, $^1J = 6.2$ Hz, 3H), 8.14–8.18 (m, 3H), 8.24 (d, $^1J = 8.1$ Hz, 2H), 8.33–8.38 (m, 3H), 8.55 (sb, 1H), 9.00 (d, $^1J = 5.2$ Hz, 2H), 9.03 ppm (d, $^1J = 5.2$ Hz, 2H); ESI-MS (CH$_3$CN): m/z: 467 $[M-2\,\text{SbF}_6]^{2+}$, 1090 $[M+\text{Cl}-\text{Py}-2\,\text{SbF}_6]^+$; conductivity: $\Lambda_\text{M}(\text{CH}_3\text{CN}) = 333 \ \Omega^{-1}\,\text{cm}^2\,\text{mol}^{-1}$; elemental analysis calcd (%) for C$_{36}$H$_{32}$F$_{18}$FeN$_5$PdSb$_3$: C 30.79, H 2.30, N 4.99; found: C 30.38, H 2.37, N 4.80.

15 ^{1}H NMR (CD$_3$CN, 27 °C, 500 MHz): $\delta = 2.32$ (s, 3H), 2.81 (s, 2H), 4.19 (s, 3H), 4.37 (t, $^1J = 1.8$ Hz, 2H), 4.40 (t, $^1J = 1.8$ Hz, 2H), 4.53 (t, $^1J = 1.8$ Hz, 2H), 4.88 (t, $^1J = 1.8$ Hz, 2H), 7.35 (d, $^1J = 5.3$ Hz, 1H), 7.59 (t, $^1J = 4.8$ Hz, 1H), 7.66 (t, $^1J = 6.3$ Hz, 1H), 7.81 (t, $^1J = 6.2$ Hz, 2H), 8.14–8.18 (m, 3H), 8.30–8.36 (m, 3H), 8.37 (d, $^1J = 8.1$ Hz, 2H), 8.54 (sb, 1H), 9.08 ppm (d, $^1J = 5.5$ Hz, 2H); ESI-MS (CH$_3$CN): m/z: 910.6 $[M-\text{SbF}_6]$; conductivity: $\Lambda_\text{M}(\text{CH}_3\text{CN}) = 267 \ \Omega^{-1}\,\text{cm}^2\,\text{mol}^{-1}$; elemental analysis calcd (%) for C$_{34}$H$_{32}$F$_{18}$FeN$_4$OPdSb$_3$: C 29.55, H 2.33, N 4.05; found: C 29.66, H 2.45, N 4.28.

Titration of 7 with TFA: A series of 0.494-mM solutions of **7** in dry CD$_3$CN containing varying amounts of dry TFA, ranging from 0.325 mM to 38.9 mM, were prepared and were examined by absorption spectrometry (25 °C). The ferrocene rotor **7** in CD$_3$CN solution is orange, and TFA is colorless. The acid–base mixtures vary in color from orange to red. The change in absorbance ($|\Delta A|$) was plotted against the number of equivalents of TFA. This plot indicated that 10 equivalents of TFA are required to fully protonate **7** (see Supporting Information). The protonation of **7** was also studied using ^{1}H NMR spectroscopy (27 °C). A series of 2.35-mM solutions of **7** in dry CD$_3$CN containing varying amounts of dry TFA, ranging from 1.59 mM to 156 mM, were prepared. The data is consistent with the results obtained by absorption spectra (see Supporting Information).

Titration of 7 with HSbF$_6$·6 H$_2$O: A series of 0.894-mM solutions of **7** in dry CD$_3$CN containing varying amounts of HSbF$_6$·6 H$_2$O, ranging from 0.356 mM to 8.54 mM, were prepared and were examined by absorption spectrometry (25 °C). The protonation of **7** with HSbF$_6$·6 H$_2$O was also studied by ^{1}H NMR spectroscopy (27 °C), and for this purpose a series of 2.94-mM solutions of **7** in dry CD$_3$CN containing varying amounts of HSbF$_6$·6 H$_2$O, ranging from 0.755 mM to 72.5 mM, were prepared. The change in absorbance or chemical shift versus the equivalents of HSbF$_6$·6 H$_2$O indicated that two equivalents of HSbF$_6$·6 H$_2$O are required to protonate **7** (see Supporting Information).

Titration of 11 with TFA and with HSbF$_6$·6 H$_2$O: The titrations of **11** with TFA and HSbF$_6$·6 H$_2$O were carried out in an analogous manner to those above. The results for the titration of **11** with TFA indicated that approximately 60 equivalents of TFA are required to fully protonate **11** (see Supporting Information). For the titration of **11** with HSbF$_6$·6 H$_2$O the changes in chemical shift were plotted against the equivalents of HSbF$_6$·6 H$_2$O; these plots indicated that 10 equivalents of HSbF$_6$·6 H$_2$O are required to fully protonate **11** (see Supporting Information).

Electrostatic repulsion calculation: The Coulombic repulsion energy for the ferrocene rotor **7** was calculated as the sum of all the cationic(+) interactions using Equation (8), in which U = electrostatic repulsion energy, e (elementary charge) = 1.602177×10^{-19} C, N_A (Avogadro constant) = 6.023×10^{23} mol^{-1}, ε_o (vacuum permittivity) = 8.85419×10^{-12} J^{-1} C^2 m^{-1}, $4\pi\varepsilon_\text{o}$ (vacuum permittivity) = 1.11265×10^{-10} J^{-1} C^2 m^{-1}, ε (dielectric constant) = 36.2 (CH$_3$CN, 298 K), 20.2 (acetone, 298 K), z (charge) = $z_\text{a} = z_\text{b} = 1+$. The charges are assumed to be point charges located at the centers of the nitrogen atoms. The cation–cation distances were obtained from molecular modeling.[31]

$$U = \frac{N_\text{A} z^2 e^2}{4\pi\varepsilon\varepsilon_0 r_\text{ab}} \qquad (8)$$

Calculated minimum cation–cation distances for the *meso* rotamer $r_\text{ab} = 3.30$ Å, and 4.10 Å for the racemic rotamer. The maximum electrostatic

repulsion energy was 2.77 kcal mol^{-1} in acetonitrile solution and 4.96 kcal mol^{-1} in acetone solution.

General procedure for crystallographic structural determinations of the ferrocene rotors

Crystallization conditions: Crystals of **7**·2(TFA) were obtained by vapor diffusion of diethyl ether into an acetonitrile solution of the ferrocene rotor **7** in the presence of 10 equivalents of TFA. Crystals of **7**·2(TfOH) were obtained by vapor diffusion of diethyl ether into an acetonitrile solution of the ferrocene rotor **7** in the presence of two equivalents of TfOH. Crystals of **7**·2(HSbF$_6$) were obtained by layering an ethanol solution containing 10 equivalents of HSbF$_6$·6 H$_2$O on top of a dichloromethane solution of **7**. Crystals of **9** were obtained by vapor diffusion of hexanes into an acetone solution of **9**. Crystals of **10** were obtained by vapor diffusion of hexanes into a dichloromethane solution of **10**. Crystals of **11** were obtained by vapor diffusion of hexanes into a dichloromethane solution of **11**. Crystals of **11**·HSbF$_6$ were obtained by layering an ethanol solution containing 10 equivalents of HSbF$_6$·6 H$_2$O on top of a dichloromethane solution of **11**. Crystals of **12** were obtained by vapor diffusion of hexanes into a dichloromethane solution of **12**. Crystals of **13** were obtained by vapor diffusion of hexanes into a dichloromethane solution of **13**. Crystals of **14** were obtained by vapour diffusion of diethyl ether into an acetonitrile solution of the **14**. Crystals of **16** were obtained by vapor diffusion of diethyl ether into an acetone solution of the both **15** and **16**, the red-brown crystals of **15** were separated from the purple crystals of **16** under a microscope. Crystals of **16** were obtained by vapor diffusion of diethyl ether into an acetonitrile solution of **16**. Crystals of **19** were obtained by vapor diffusion of hexanes into a dichloromethane solution of **19** (see Supporting Information).

Data collection: A suitable crystal was selected under a stereo-microscope while immersed in Fluorolube oil to avoid possible reaction with air. The crystal was removed from the oil using a tapered glass fiber that also served to hold the crystal for data collection. The crystal was mounted and centered on a Bruker SMART APEX system at 100 K. Still images showed the diffractions to be sharp. Frames separated in reciprocal space were obtained and provided an orientation matrix and initial cell parameters. Final cell parameters were obtained from the full data set.

A "full sphere" data set was obtained which samples approximately all of reciprocal space to a resolution of 0.75 Å using 0.3° steps in ω using 10 s integration times for each frame. Data collection was made at 100 K. Integration of intensities and refinement of cell parameters were done using SAINT.[32] Absorption corrections were applied using SADABS[32] based on redundant diffractions.

Structure solution and refinement: The space group of the crystal was determined based on systematic absences and intensity statistics. Direct methods were used to locate the Fe and the other heavy atoms (such as Pd and Sb), and most C atoms from the E-map. Repeated difference Fourier maps allowed recognition of all expected atoms. The N assignments were based on the abnormal small thermal parameter on the originally assigned C atoms. Following anisotropic refinement of all non-H atoms, ideal H atom positions were calculated. Final refinement was anisotropic for all non-H atoms isotropic-riding for H atoms. Except for slight disorder in some of the SbF$_6^-$ groups, no anomalous bond lengths or thermal parameters were noted for the molecules. All ORTEP diagrams have been drawn with 50 % probability ellipsoids.

CCDC-271205 (**7**·2(HSbF$_6$)), CCDC-268421 (**9**), CCDC-268429 (**10**), CCDC-268425 (**11**), CCDC-270740 (**11**·HSbF$_6$), CCDC-268415 (**12**), CCDC-268428 (**13**), CCDC-268423 (**14**), CCDC-268427 (**16**), CCDC-268424 (**15**) contain the supplementary crystallographic data for this paper. These data can be obtained free of charge from The Cambridge Crystallographic Data Centre via www.ccdc.cam.ac.uk/data_request/cif.

[1] a) A. Houdusse, H. L. Sweeney, *Curr. Opin. Struct. Biol.* **2001**, *11*, 182–194; b) A. F. Huxley, *Philos. Trans. R. Soc. London Ser. B* **2000**, *355*, 433–440; c) F. J. Kull, S. A. Endow, *J. Cell Sci.* **2002**, *115*, 15–23; d) D. Stock, A. G. Leslie, J. E. Walker, *Science* **1999**, *286*, 1700–1705; e) A. Yildiz, M. Tomishige, R. D. Vale, P. R. Selvin, *Science* **2004**, *303*, 676–678; f) C. L. Asbury, A. N. Fehr, S. M. Block, *Science* **2003**, *302*, 2130–2134; g) W. Hua, J. Chung, J. Gelles, *Science* **2002**, *295*, 844–848; h) R. A. Cross, *Curr. Biol.* **2004**, *14*, R158–R159.

[2] a) M. Yoshida, E. Muneyuki, T. Hisabori, *Nat. Rev. Mol. Cell Biol.* **2001**, *2*, 669–677; b) G. Oster, H. Wang, *Biochim. Biophys. Acta* **2000**, *1458*, 482–510; c) P. D. Boyer, *Annu. Rev. Biochem.* **1997**, *66*, 717–749; d) P. Dimroth, *Biochim. Biophys. Acta* **2000**, *1458*, 374–386; e) T. C. Elston, G. Oster, *Biophys. J.* **1997**, *73*, 703–721; f) H. C. Berg, *Philos. Trans. R. Soc. London Ser. B* **2000**, *355*, 491–501; g) D. J. Derosier, *Cell* **1998**, *93*, 17–20.

[3] a) *Molecular Motors* (Ed.: M. Schliwa), Wiley-VCH, Weinheim, **2003**; b) M. Schliwa, G. Woehlke, *Nature* **2003**, *422*, 759–765; c) K. Kinbara, T. Aida, *Chem. Rev.* **2005**, *105*, 1377–1400.

[4] a) G. Oster, H. Wang, *Molecular Motors* (Eds.: M. Schliwa), Wiley-VCH, Weinheim, **2003**, chap. 8, p. 207; b) G. Oster, H. Wang, *Trends Cell Biol.* **2001**, *11*, 196–202; c) G. Oster, H. Wang, *Appl. Phys. A* **2002**, *75*, 315–323; d) P. Reimann, *Phys. Rep.* **2002**, *361*, 57–265.

[5] a) R. A. Bissel, E. Córdova, A. E. Kaifer, J. F. Stoddart, *Nature* **1994**, *369*, 133–137; b) P. R. Ashton, R. Ballardini, V. Balzani, I. Baxter, A. Credi, M. C. T. Fyfe, M. T. Gandolfi, M. Gomez-Lopez, M.-V. Martinez-Diaz, A. Piersanti, N. Spencer, J. F. Stoddart, M. Venturi, A. J. P. White, D. J. Williams, *J. Am. Chem. Soc.* **1998**, *120*, 11932–11942; c) J. D. Badjic, V. Balzani, A. Credi, S. Silvi, J. F. Stoddart, *Science*, **2004**, *303*, 1845–1849; d) F. Ibukuro, T. Kusukawa, M. Fujita, *J. Am. Chem. Soc.* **1998**, *120*, 8561–8562; e) J. D. Crowley, A. J. Goshe, I. M. Steele, B. Bosnich, *Chem. Eur. J.* **2004**, *10*, 1944–1955.

[6] a) W-Y. Sun, T. Kusukawa, M. Fujita, *J. Am. Chem. Soc.* **2002**, *124*, 11570–11571; b) M. Asakawa, P. R. Ashton, V. Balzani, A. Credi, C. Hamers, G. Mattersteig, M. Montalti, A. N. Shipway, N. Spencer, J. F. Stoddart, M. S. Tolley, M. Venturi, A. J. P. White, D. J. Williams, *Angew. Chem.* **1998**, *110*, 357–361; *Angew. Chem. Int. Ed.* **1998**, *37*, 333–337; c) V. Balzani, J. Becher, A. Credi, M. B. Nielsen, F. M. Raymo, J. F. Stoddart, A. M. Talarico, M. Venturi, *J. Org. Chem.* **2000**, *65*, 1947–1956.

[7] a) D. A. Leigh, J. K. Y. Wong, F. Dehez, F. Zerbetto, *Nature* **2003**, *424*, 174–179; b) A. M. Brouwer, C. Frochot, F. G. Gatti, D. A. Leigh, L. Mottier, F. Paolucci, S. Roffia, G. W. Wurpel, *Science* **2001**, *291*, 2124–2128; c) N. Koumura, R. W. J. Zijistra, R. A. Van Delden, N. Harada, B. L. Feringa, *Nature* **1999**, *401*, 152–155; d) T. Muraoka, K. Kinbara, Y. Kobayashi, T. Aida, *J. Am. Chem. Soc.* **2003**, *125*, 5612–5613; e) F. M. Hawthorne, J. I. Zink, J. M. Skelton, M. J. Bayer, C. Liu, E. Livshits, R. Baer, D. Neuhauser, *Science* **2004**, *303*, 1849–1851; f) J. V. Hernandez, E. R. Kay, D. A. Leigh, *Science* **2004**, *306*, 1532–1537; g) Y. Liu, A. H. Flood, P. A. Bonvallet, S. A. Vignon, H.-R. Tseng, T. J. Huang, B. Brough, M. Baller, S. Magonov, S. Solares, W. A. Goddard, C.-M. Ho, J. F. Stoddart, *J. Am. Chem. Soc.* **2005**, *127*, 9745–9759.

[8] a) V. Balzani, M. Venturi, A. Credi, *Molecular Devices and Machines*, Wiley-VCH, Weinheim, **2003**; b) V. Balzani, A. Credi, F. M. Raymo, J. F. Stoddart, *Angew. Chem.* **2000**, *112*, 3486–3531; *Angew. Chem. Int. Ed.* **2000**, *39*, 3349–3391; c) M. C. Jimenez-Molero, C. Dietrich-Buchecker, J.-P. Sauvage, *Chem. Commun.* **2003**, *14*, 1613–1616; d) Molecular machines special issue (Ed.: J. F. Stoddart), *Acc. Chem. Res.* **2001**, *34*, 409–522; e) E. R. Kay, D. A. Leigh in *Functional Artificial Receptors* (Eds.: T. Schrader, A. D. Hamilton), Wiley-VCH, Weinheim, **2005**, pp. 333–406; f) E. R. Kay, D. A.

Leigh, *Top. Curr. Chem.* **2005**, *262*, 133–177; g) G. S. Kottas, L. I. Clarke, D. Horinek, J. Michl, *Chem. Rev.* **2005**, *105*, 1281–1376; h) S. P. Fletcher, F. Dumur, M. M. Pollard, B. L. Feringa, *Science* **2005**, *310*, 80–82.

[9] A. Haaland, *Acc. Chem. Res.* **1979**, *12*, 415–422.

[10] S. Carter, J. N. Murrell, *J. Organomet. Chem.* **1980**, *192*, 399–408.

[11] a) P. Seiler, J. D. Dunitz, *Acta Crystallogr. Sect. B* **1979**, *35*, 2020–2032; b) P. Seiler, J. D. Dunitz, *Acta Crystallogr. Sect. B* **1979**, *35*, 1068–1074; c) J. D. Dunitz, L. E. Orgel, A. Rich, *Acta Crystallogr.* **1956**, *9*, 373–375; d) J. D. Dunitz, L. E. Orgel, *Nature* **1953**, *171*, 121–122.

[12] T. N. Doman, C. R. Landis, B. Bosnich, *J. Am. Chem. Soc.* **1992**, *114*, 7264–7272.

[13] ConQuest, 1.4; software for searching the Cambridge Crystallographic Data Centre's database of crystal structures, http:// www.ccdc.cam.ac.uk; The Cambridge Crystallographic Data Centre: UK, **2004**.

[14] a) F. Gelin, R. P. Thummel, *J. Org. Chem.* **1992**, *57*, 3780–3783; b) A. Kasahara, T. Izumi, Y. Yoshida, I. Shimizu, *Bull. Chem. Soc. Jpn.* **1982**, *55*, 1901–1906; c) I. Shimizu, H. Umezawa, T. Kanno, T. Izumi, A. Kasahara, *Bull. Chem. Soc. Jpn.* **1983**, *56*, 2023–2028; d) I. Shimizu, Y. Kamei, T. Tezuka, T. Izumi, A. Kasahara, *Bull. Chem. Soc. Jpn.* **1983**, *56*, 192–198.

[15] M. Inouye, Y. Hyodo, H. Nakazumi, *J. Org. Chem.* **1999**, *64*, 2704–2710.

[16] a) C. Janiak, *J. Chem. Soc. Dalton Trans.* **2000**, 3885–3896; b) C. A. Hunter, K. R. Lawson, J. Perkins, C. J Urch, *J. Chem. Soc. Perkin Trans. 2* **2001**, 651–669.

[17] a) S. Barlow, A. Cowley, J. C. Green, T. J. Brunker, T. Hascall, *Organometallics* **2001**, *20*, 5351–5359; b) A. A. Koridze, N. M. Astakhova, P. V. Petrovskii, *J. Organomet. Chem.* **1983**, *254*, 345–360; c) A. Ceccon, G. Giacometti, A. Venzo, D. Paolucci, D. Benozzi, *J. Organomet. Chem.* **1980**, *185*, 231–239; d) J. J. Dannenberg, M. K. Levenberg, J. H. Richards, *Tetrahedron* **1973**, *29*, 1575–1584.

[18] a) M. Rosenblum, J. O. Santer, *J. Am. Chem. Soc.* **1959**, *81*, 5517–5518; b) U. T. Mueller-Westerhoff, T. J. Haas, G. F. Swiegers, T. K. Leipert, *J. Organomet. Chem.* **1994**, *472*, 229–246; c) G. Cerichelli, G. Illuminati, G. Ortaggi, A. M. Giuliani, *J. Organomet. Chem.* **1977**, *127*, 357–370.

[19] F. Tran, J. Weber, T. A. Wesolowski, *Helv. Chim. Acta* **2001**, *84*, 1489–1503.

[20] J. R. Grover, E. A. Walters, E. T. Hui, *J. Phys. Chem.* **1987**, *91*, 3233–3237.

[21] R. Knapp, M. Rehahn, *J. Organomet. Chem.* **1993**, *452*, 235–240.

[22] a) D. Braga, M. Polito, M. Bracaccini, D. D'Addario, E. Tagliavini, L. Sturba, F. Grepioni, *Organometallics* **2003**, *22*, 2142–2150; b) D. Braga, M. Polito, M. Bracaccini, D. D'Addario, E. Tagliavini, D. M. Proserpio, F. Grepioni, *Chem. Commun.* **2002**, 1080–1081.

[23] S. Doherty, E. G. Robins, I. Pal, C. R. Newman, C. Hardacre, D. Rooney, D. A. Mooney, *Tetrahedron: Asymmetry* **2003**, *14*, 1517–1527.

[24] B. H. Han, D. H. Shin, S. Y. Cho, *Tetrahedron Lett.* **1985**, *26*, 6233–6234.

[25] K. Izutsu, *Acid-Base Dissociation Constants in Dipolar Aprotic Solvents*, Blackwell, London, **1990**.

[26] W. J. Geary, *Coord. Chem. Rev.* **1971**, *7*, 81–122.

[27] X.-B. Wang, D. Bing, H.-K. Woo, L.-S. Wang, *Angew. Chem.* **2005**, *117*, 6176–6178; *Angew. Chem. Int. Ed.* **2005**, *44*, 6022–6024.

[28] T. Muraoka, K. Kinbara, T. Aida, *Nature* **2006**, *440*, 512–515.

[29] Y-Q. Fang, G. S. Hanan, *Synlett* **2003**, 852–854.

[30] F. S. Kamounah, J. B. Christensen, *J. Chem. Res. Synop.* **1997**, 150.

[31] PC Spartan Pro, Version 1.0.5, **1999**, Wavefunction, Irvine, CA.

[32] G. Sheldrick, SHELXTL (version 6.1) program library; G. Bruker Analytical X-ray Systems, Madison, WI, **2000**.